ARTICLE IN PRESS

Available online at www.sciencedirect.com

ScienceDirect

Geochimica et Cosmochimica Acta xxx (2020) xxx–xxx

Geochimica et Cosmochimica Acta

www.elsevier.com/locate/gca

NanoSIMS isotopic investigation of xenolithic carbonaceous clasts from the kapoeta howardite

Nan Liu *, Ryan C. Ogliore, Lionel G. Vacher

Laboratory for Space Sciences and the Department of Physics, Washington University in St. Louis, St. Louis, MO 63130, USA

Received 27 February 2020; accepted in revised form 23 May 2020; available online xxxx

Abstract

We report on the investigation of presolar grains and organic matter (OM) in 14 xenolithic carbonaceous clasts (C-clasts) identified in the Kapoeta howardite based on high-resolution NanoSIMS hydrogen, carbon, nitrogen, and oxygen isotopic imaging data. The 14 C-clasts are ~50–200 μm in size and consist of one CM-like and 13 CI-like clasts, which are classified based on their mineralogies. The clasts from this study are likely sourced from an ice-bearing parent body, either an icy asteroid or a comet, originating from the outer solar system according to the following mineralogical observations: (1) in two CI-like clasts, embayments of magnetite grains between the C-clast and the host howardite point to aqueous alteration occurring on Vesta as a result of melting the ice embedded in the C-clasts; (2) all of the C-clasts, especially the 13 CI-like clasts, likely originated from the same parent body, because (i) the 14 C-clasts are clustered in the thin section, and (ii) the clasts show a much higher ratio of CI-like to CM-like clasts with respect to those reported in the literature. Four presolar silicon carbide (SiC) and two presolar silicate grains were identified in the C-clasts. In addition, all the C-clasts contain moderate bulk D- and ^{15}N-enrichments with the presence of sub-micron to micron-sized D and ^{15}N hotspots, indicating the presence of primitive organic material. Comparison of the abundances and isotopic compositions of presolar grains and OM in these C-clasts with literature data for different samples of primitive extraterrestrial material provides support for (1) the genetic linkage of xenolithic C-clasts to highly aqueously altered but minimally heated carbonaceous chondritic materials and (2) a homogeneous distribution of circumstellar and interstellar materials in the protoplanetary disk. The low amounts of heat experienced by the C-clasts suggest that they arrived at Vesta and/or Vestoids at low speeds after the late heavy bombardment in the inner solar system ~3.5–4.0 Gyr ago.

Keywords: Carbonaceous chondrite; Vesta; Howardite Kapoeta; NanoSIMS; Isotopic anomalies; Presolar grains; Organic matter

1. INTRODUCTION

The Dawn mission revealed that asteroid 4 Vesta, the second largest body in the asteroid belt, is differentiated with an iron-rich core, a silicate mantle, and a basaltic crust (De Sanctis et al., 2012). The Dawn mission observations also provide strong support for the proposal that Vesta is the parent body of HED (howardite, eucrite, and diogenite) meteorites (De Sanctis et al., 2012), the most abundant type of achondrites in our meteorite collection (Mittlefehldt, 1997). Among HED meteorites, howardites are achondritic brecciated mixtures of diogenites, eucrites, and other components (e.g., Pun et al., 1998) including carbonaceous chondrite clasts (C-clasts hereafter) that contain phyllosilicates, carbonates, and other minerals that formed by aqueous alteration (Wilkening 1973; Buchanan et al., 1993; Zolensky et al., 1996; Gounelle et al., 2003). The differentiation of Vesta likely started within 1 Myr after the injection of ^{26}Al into the young solar system and lasted for ~10 Myr before the solidification of Vesta (Formisano et al., 2013; Weisfeiler et al., 2017). C-clasts in howardites were likely

* Corresponding author.

https://doi.org/10.1016/j.gca.2020.05.026
0016-7037/

trapped in the regolith after the differentiation of Vesta but before the lithification of the regolith (Gounelle et al., 2003).

The presence of C-clasts in howardites (Wilkening, 1973; Zolensky et al., 1992; Buchanan et al., 1993; Metzler et al., 1995; Pun et al., 1998; Gounelle et al., 2003, 2005; Bishcoff et al., 2006; Lorenz et al., 2007; Patzek et al., 2018a) is not unique. Primitive xenolithic C-clasts have also been observed in other classes of meteorites, including ureilites (Brearley and Prinz, 1992; Ikeda et al., 2000; Goodrich et al., 2004, 2009; Bischoff et al., 2006; Patzek et al., 2018a, 2020; Visser et al., 2018), ordinary chondrites (Fodor and Keil, 1976; Keil et al., 1980; Nozette and Wilkening, 1982; Rubin, 1989; Rubin and Bottke, 2009; Kebukawa et al., 2017; Patzek et al., 2018a; Bischoff et al., 2018), R chondrites (Greshake, 2014; Patzek et al., 2018a), and aubrites (Lorenz et al., 2005). The presence of xenolithic C-clasts in different classes of meteorites that originated from different parent bodies strongly indicates that carbonaceous-chondrite-like micrometeoroids were widespread in the early solar system (Gounelle et al., 2003).

The source of xenolithic C-clasts remains enigmatic. Mineralogical and petrologic characterization of C-clasts shows that they are similar to CM and CI chondrites (Patzek et al., 2018a) that are thought to originate from asteroids. Given the small sizes of C-clasts, it is difficult to obtain precise bulk oxygen isotopic data to definitively confirm the linkage between CM-like and CI-like clasts with CM and CI chondrites, respectively. This is particularly true in the case of CI material because of its highly brecciated nature (Morlok et al., 2006; Alfing et al., 2019). Oxygen isotope data were obtained for a few CM-like and CI-like clasts in the literature (Brearley and Prinz, 1992; Patzek et al., 2018b), which suggests similarities between CM-like clasts and CM chondrites, and differences between CI-like clasts and CI chondrites. The investigated CI-like clasts, however, were all from ureilites and may represent a distinct group of CI-like clasts with respect to CI-like clasts from other groups of meteorites, as recently suggested by Patzek et al. (2020). The ratio of D/H has been determined for a number of C-clasts of both types from different meteorites (Gounelle et al., 2005; Patzek et al., 2020). There are, however, significant overlaps in the D/H ratio among different meteorite groups and also between CM-like and CI-like clasts, although CI-like clasts from CR chondrites and ureilites generally exhibit much larger D excesses (Patzek et al., 2020). Intriguingly, observations showed that in larger millimeter-sized clasts found in howardites, CM-like clasts are more abundant than CI-like C-clasts, whereas the opposite is true for smaller C-clasts (Zolensky et al., 1996; Gounelle et al., 2003). The observed size-dependent differences, therefore, suggest that smaller C-clasts are not fragments of larger bodies disrupted in violent impacts (Zolensky et al., 1996; Gounelle et al., 2003).

C-clasts in howardites and other meteorites are well-preserved samples of primitive solar system material. Carbonaceous micrometeoroids must have impacted their parent asteroids at relatively low speeds, since the C-clasts are intact and were not significantly heated (Gounelle et al., 2003; Rubin and Bottke, 2009). The peak temperature of both CM-like and CI-like clasts is constrained to lie below ~100 °C from Raman spectroscopy (Visser et al., 2018). This is in general agreement with the low temperatures inferred from their mineralogies (Zolensky et al., 1996). Xenolithic C-clasts, therefore, provide us a unique opportunity to study pristine and primordial solar system solids, including possible cometary material, which fell onto other bodies in the early solar system and thus may be distinct from carbonaceous meteorites, micrometeorites, and interplanetary dust particles (IDPs) that fall to Earth today.

Micro C-clasts, micrometeorites, and IDPs – submillimeter extraterrestrial materials –likely represent samples sourced from different parent-body populations and at different times. Given their short residence lifetimes on Earth (e.g., Prasad et al., 2013; Jull, 2001), micrometeorites are likely representative samples of submillimeter particles in the present-day zodiacal cloud at 1 AU, which is predicted to consist mostly of material from Jupiter-family comets (Nesvorný et al., 2010). In comparison, micro C-clasts could be ancient samples that have been implanted into their intermediary parent asteroids, i.e., the secondary parent bodies on which micro C-clasts resided prior to their arrival on Earth, billions of years ago (e.g., Gounelle et al., 2003). Dynamic models predict that submillimeter dust of both cometary and asteroidal origins could have been implanted onto Vesta at low speeds (Briani et al., 2011). However, so far no evidence has been observed to distinguish between cometary and asteroidal micro C-clasts in howardites. The lack of two distinct groups led to the proposal that there is a continuum in the chemical and mineralogical properties between asteroidal and cometary dust (Briani et al., 2011). This proposal is consistent with the observation that the ~10-μm rocky component of comet Wild 2 consists mainly of high-temperature minerals that are commonly found in meteorite samples from asteroids (Brownlee et al., 2012). In addition, numerical simulations suggest that C-type and a portion of P- and D-type asteroids originally formed in the outer solar system as comets (Levison et al., 2009; Walsh et al., 2011), such that significant overlap could exist between these asteroids and comets in their chemical and mineralogical properties. Based on spectral properties, it has been proposed that while olivine-rich IDPs are likely to have been sourced from comets, a large fraction of less olivine-rich IDPs with diverse mineralogies could represent samples of icy asteroids, which are about 60 % of the mass of the main asteroid belt (Vernazza et al., 2015).

Given their fine-grained and primitive nature, xenolithic C-clasts may host abundant presolar grains and primitive organic matter (OM). Presolar grains represent circumstellar materials that were incorporated into the molecular cloud prior to the formation of the solar system and survived early solar system processing (Zinner, 2014; Nittler and Ciesla, 2016). They are characterized by large isotopic anomalies that represent the nucleosynthetic signatures of their parent stars. Primitive OM also exhibits large isotopic anomalies but mainly in the volatile elements, hydrogen and nitrogen (Messenger et al., 2003; Busemann et al., 2006). The large D- and ^{15}N-enrichments observed in OM have been ascribed to large isotope fractionation caused by chemistry occurring at extremely low temperatures in the interstellar medium (ISM), the parent molecular cloud, and/or the cold outer regions of the solar protoplanetary disk (e.g., Alexander et al., 1998; Messenger 2000; Aikawa et al., 2002). Xenolithic C-clasts in meteorites can thus help constrain the inventories of presolar materials in the solar nebula, since some clasts might otherwise not be represented in the meteorite record (e.g., Nittler et al., 2019a).

In addition, presolar materials in these clasts can be used to probe the secondary processes (Huss et al., 2003; Floss and Haenecour, 2016) that these C-clasts experienced on their original parent bodies as well as on their intermediary parent bodies prior to their arrival on Earth. Extensive in situ surveys of primitive meteorites have shown that the abundance of presolar grains and the isotopic composition of OM vary widely among different meteorite groups and petrologic types, largely reflecting the degree of secondary processing (e.g., aqueous alteration, thermal metamorphism) experienced by the host meteorite (Floss and Haenecour, 2016; Alexander et al., 2007, 2017). In detail, silicates are the most abundant type of presolar grains identified in situ in primitive chondrites with a matrix-normalized abundance of up to ~200 ppm in unequilibrated chondrites (e.g., Floss and Stadermann, 2009; Nittler et al., 2018). Higher abundances of presolar silicates were observed in anhydrous IDPs of possible cometary origin collected in the stratosphere (Messenger et al., 2003; Floss et al., 2006). Compared to anhydrous IDPs, the reduced presolar silicate abundances observed in the most primitive chondrites are interpreted as a result of slight parent body processing (Floss and Haenecour, 2016). Alternatively, it could reflect a heterogeneous distribution of presolar silicates in the protoplanetary disk – presolar silicates may be more abundant in the comet-forming region. In addition, significantly lower abundances of presolar silicates have been observed in meteorites (CM2, CR2) that experienced aqueous alteration (e.g., Leitner et al., 2012, 2019; Nittler et al., 2019b). In this case, the lowered abundances likely resulted from altering labile presolar silicates or reequilibrating their oxygen isotopic compositions by exchange with a fluid (Floss and Haenecour, 2016).

Another presolar mineral phase, silicon carbide (SiC), is quite resistant to aqueous alteration but labile to thermal metamorphism (Huss and Lewis, 1995). An abundance of ~30 ppm presolar SiC has been observed in a number of CI, CR, and CM meteorites (Davidson et al., 2014a). In comparison, lower abundances of presolar SiC grains were found in CO, CV, and ordinary chondrites of high petrologic types, likely resulting from oxidation and, in turn, destruction of SiC at high temperatures because of parent body thermal metamorphism (Huss and Lewis, 1995; Huss et al., 2003; Davidson et al., 2014a). Finally, it was shown that loss of D-rich OM could occur, even if the parent body experienced a low degree of thermal metamorphism (Nittler et al., 2018). This is also supported by the fact that insoluble OM, the most abundant form of primitive OM in CV and CO chondrites that generally experienced peak temperatures above ~200 °C (e.g., Bonal et al., 2016), shows smaller D excesses compared to those from CI, CM, and CR meteorites that generally experienced less heating (Alexander et al., 2007). Thus, the abundances and isotopic compositions of presolar grains and OM in C-clasts from howardites can be used to trace the degree of secondary processing experienced by the C-clasts on both their parent bodies and Vesta. This information can also be used to explore heterogeneity in the distributions of circumstellar and interstellar materials across the solar system. Here, we present the first systematic NanoSIMS isotopic investigation (H, C, N, O, Si) of xenolithic C-clasts from the Kapoeta howardite at high spatial resolution.

2. METHODS

2.1. Petrologic characterization

We obtained a polished thin section of Kapoeta (USNM 67331) from the Smithsonian Museum. The thin section was first characterized by using a Tescan Mira3 FEG-SEM at Washington University in St. Louis. We obtained ~12,000 backscattered electron (BSE) images (50 μm field-of-view) across the sample, from which we identified 15 C-clasts ~50–200 μm in size. The clasts were named in the format of xxx (column number of the BSE image mosaic)-yyy (row number). We then acquired energy dispersive X-ray maps of these C-clasts for qualitative phase analyses. The locations of the identified C-clasts and BSE images of two C-clasts are shown in Fig. 1. Note that we did not obtain any NanoSIMS data for one of the 15C-clasts (located on the lower right side of C-clast 060–005 in supplement) and will not discuss it further. However, since this C-clast belongs to the CM-like type, we will include it when discussing the ratio of CI- to CM-like C-clasts in Section 4.1.

2.2. NanoSIMS isotopic imaging

We analyzed 14 of the 15 identified C-clasts by isotopic imaging with the Cameca NanoSIMS 50 ion microprobe at Washington University in St. Louis. We adopted the methods used previously for presolar grain and organic mapping of meteorite thin sections (Floss and Stadermann, 2009, 2012). For identifying presolar carbon- and oxygen-rich grains, we rastered a ~ 1 pA focused Cs^+ primary ion beam of 16 keV over 10 × 10 μm areas with simultaneous collection of $^{12}C^-$, $^{13}C^-$, $^{16}O^-$, $^{17}O^-$, and $^{18}O^-$ along with secondary electrons at a spatial resolution of ~100–150 nm. Prior to image acquisition, areas were pre-sputtered for roughly 30 min with a ~ 100 pA beam to remove the C coat over 12 × 12 μm areas. A hundred sequential 256 × 256 pixel cycles were acquired on each area for a total acquisition time of 2 hr. We searched for presolar grains using the L'image software (from Dr. Larry Nittler, see Nittler et al., 2018 for details). The L'image software was used to correct for the deadtime effect of the electron multiplier counting system, shifts between image frames, and quasi-simultaneous arrival effects (Slodzian et al., 2014). The

ARTICLE IN PRESS

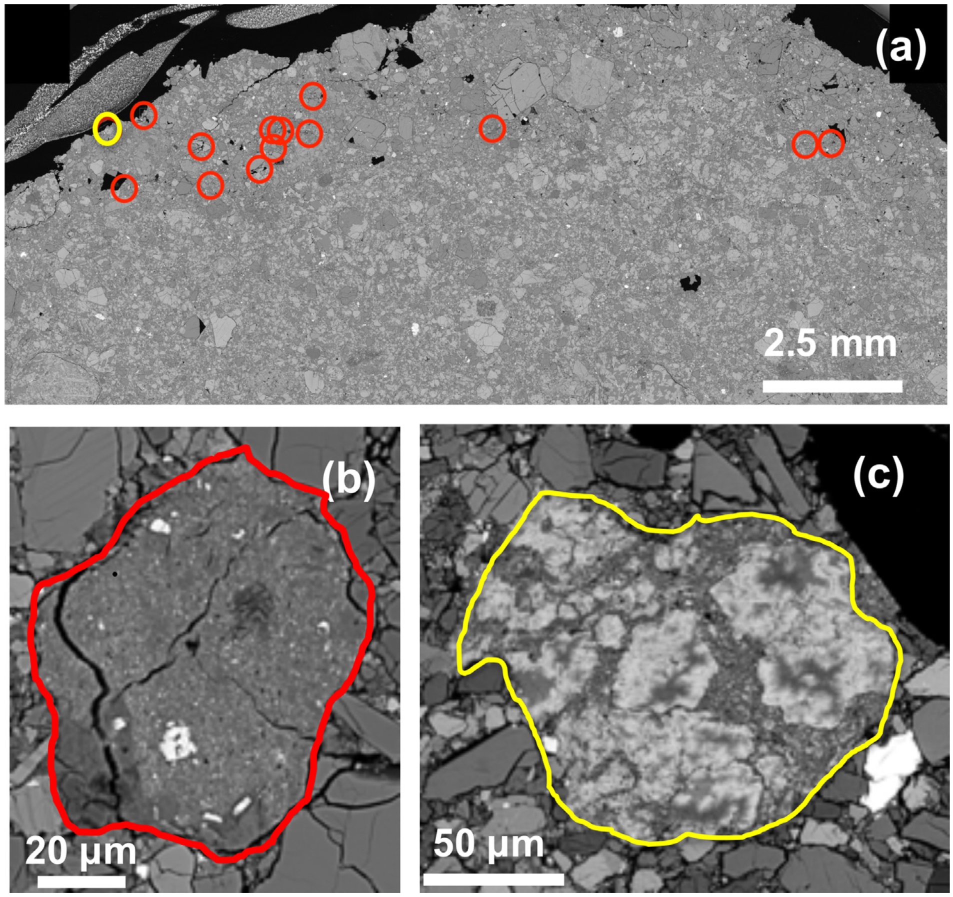

Fig. 1. (a) BSE overview image of USNM 67331 thin section from Kapoeta meteorite. Yellow and red circles denote the CM-like and CI-like C-clasts, respectively, identified in this study. Examples of a CI-like and CM-like C-clast (highlighted by lines with corresponding colors) are shown in (b) and (c), respectively, in BSE images. (For interpretation of the references to colour in this figure legend, the reader is referred to the web version of this article.)

identified carbon-anomalous grains were further analyzed for nitrogen and silicon isotopes by acquiring their $^{12}C^{14}N^-$, $^{12}C^{15}N^-$, $^{28}Si^-$, $^{29}Si^-$, $^{30}Si^-$ ion images in 3×3 µm areas.

In addition, we selected three C-clasts that contain presolar grains for further investigation of their isotopic compositions of hydrogen, carbon, and nitrogen of OM. We first rastered a ~ 1 pA Cs^+ beam over 10×10 µm areas with simultaneous collection of $^{12}C^-$, $^{13}C^-$, $^{12}C^{14}N^-$, $^{12}C^{15}N^-$, and $^{28}Si^-$, and then a ~ 3 pA Cs^+ beam over the same areas with simultaneous collection of $^1H^-$ and $^2H^-$. The increased beam current for hydrogen isotope analyses resulted in a degraded spatial resolution of ~200–250 nm. The analysis time was 4 hr for each area in both NanoSIMS sessions.

For all measurements, the mass resolving power was 7,000–9,000, sufficient to resolve (<1 % contribution) potential isobaric interferences ($^{16}OH^-$ on $^{17}O^-$, $^{13}C_2^-$ on $^{12}C^{14}N^-$, $^{28}SiH^-$ on $^{29}Si^-$). Carbon, oxygen and nitrogen isotopes were internally normalized to the average composition of each image, while H isotopes were normalized to epoxy infilling cracks in the thin section, which were assumed to have terrestrial composition. For the nitrogen and silicon isotope measurements of identified carbon-anomalous grains, synthetic SiC and Si_3N_4 were measured for standardization.

2.3. Auger Electron Spectroscopy

We analyzed the major element compositions of oxygen-anomalous grains with the PHI 700 Auger nanoprobe at Washington University in St. Louis, using the established procedures for presolar silicate grains (Stadermann et al., 2009; Floss, 2018). We acquired both imaging and spectral data on each grain at a spatial resolution of ~20 nm. For data reduction, we adopted the previously reported sensitivity factors for oxygen, magnesium, aluminum, silicon, calcium, and iron that were determined from olivine and pyroxene standards of various compositions (Stadermann et al., 2009). The carbon-anomalous grains were not analyzed with Auger, because three of the four identified grains were consumed during the NanoSIMS nitrogen and silicon isotopic characterization, according to their decreasing ion signals during the analyses.

3. RESULTS

3.1. Mineralogy of C-clasts in kapoeta

Fig. 1 shows that the fine-grained xenolithic C-clasts can be easily distinguished from the coarse-grained anhydrous components in the howardite host in BSE images. The comparison given in Table 1 shows that the clasts from this study are quite similar mineralogically to those from Patzek et al. (2018a) mineralogically. According to the petrology-based-classification scheme of Patzek et al. (2018a), 13 of the 14 C-clasts belong to CI-like and only one CM-like C-clast with the former being rich in sulfides and magnetite and the latter rich in mixed tochilinite-serpentine phases. In addition, based on the energy dispersive X-ray spectroscopy (EDS) data obtained with our SEM (standards-based eZAF quantification), it suggests that these C-clasts contain 1–4 wt.% carbon, which is consistent with those reported for CI and CM chondrites (Pearson et al., 2006; Alexander et al., 2012; Vacher et al., 2020) and thus supports their classification as CI- and CM-like materials.

The CM-like clast is ~150 μm in size and contains abundant clumps of Fe, S-rich phyllosilicates (Fig. 1c), probably made of tochilinitie-cronstedtite intergowth (TCI). Its separation from the host meteorite is distinct, and no sign of aqueous alteration is observed in the surrounding howardite silicates. Compared to the CM-like clast, the 13 CI-like clasts are smaller (<100 μm) and are dominated by a heterogenous fine-grained matrix free of phyllosilicate clumps. Out of the 13 CI-like clasts, 12 clasts contain significant amounts of magnetite grains with various types of morphologies: (1) framboids with an average crystal size of ~1 μm (Fig. 7a – d), (2) aggregates of anhedral crystals up to ~5 μm in size (Fig. 7e), (3) isolated subhedral crystals of various size (1–5 μm), and (4) plaquettes ~5 μm in size (see supplement). Additionally, a few CI-like clasts also contain rare, isolated grains of forsterite ($Fo_{91\text{-}99}$) up to ~10 μm in size (Fig. 7a) and Fe, Ni-sulfide (mostly pyrrhotite) 1–5 μm in size (Fig. 7c). In the CI-like clast 039–007, no magnetite grains are present. Instead, this clast contains numerous small grains of Ca-carbonates (~5 μm), pentlandite (1–3 μm), and a fine-grained phyllosilicate-rich matrix (see supplement). The CI-like clasts are often delimited by surrounding fractures that separate them from their howardite host.

3.2. Presolar grains

A total area of 15,216 μm^2 of fine-grained matrix-like clast material in all 14 clasts was searched for carbon- and oxygen-anomalous presolar grains. Presolar oxygen-rich and carbon-rich grain candidates were first identified by manual examination of the isotope ratio images and then confirmed if at least one isotope ratio of carbon or oxygen was $> 5.3\sigma$ away from the surrounding meteorite matrix (Hoppe et al., 2015; Leitner et al., 2019). As shown by Hoppe et al. (2015), the often adopted 4σ criterion is not necessarily sufficient for the identification of presolar grains, since in addition to counting statistics, variations in the measured isotope ratios can also be caused by other factors like topography, local charging or ion bombardment. This way, we identified three oxygen-anomalous grains and four carbon-anomalous grains (Table 2), and their corresponding isotopic compositions are summarized in Tables 3 and 4, respectively. Following the procedure of Nittler et al. (2018), the isotope ratios were calculated by including all pixels within the full width at half maximum of "sigma" images given in the L'image software. In the "sigma" images, each pixel represents the number of standard deviations its measured isotope ratio is from the terrestrial ratio. The isotope ratios are reported with 1σ errors in the form of either absolute ratios or delta values, which are deviations from a standard ratio in per mil and defined as $\delta R = (R_{measured}/R_{standard} - 1) \times 1000$. The $R_{standard}$ ratios for δD, $\delta^{12}C$, $\delta^{15}N$, $\delta^{29}Si$ and $\delta^{30}Si$ are D/H, $^{12}C/^{13}C$, $^{15}N/^{14}N$, $^{29}Si/^{28}Si$ and $^{30}Si/^{28}Si$, respectively. The grain areas for oxygen-anomalous grains were determined from the high-resolution secondary electron (SE) images obtained with the Auger nanoprobe. Since three of the four carbon-anomalous grains were totally consumed during the N-Si isotope characterization, we could not obtain high-resolution SE images of the grains afterwards. As a result, the sizes of carbon-anomalous grains were determined from the NanoSIMS secondary ion images, which likely overestimated the grain sizes because of the ~100–150 nm primary beam size.

3.2.1. Presolar oxygen-rich grains

Our Auger elemental data show that oxygen-anomalous grains 039-007-1 and 022-005-1 are Mg, Fe-rich silicates and grain 022–005-2 is an Fe, Al-rich oxide (Fig. 2). Their oxygen isotopic data are compared to the literature data for presolar oxides and silicates (presolar grain database, Hynes and Gyngard, 2009) in Fig. 3. Fig. 3a shows that presolar oxygen-rich grains have been divided into four groups based on their oxygen isotopic compositions (Nittler et al., 1997, 2008). The two presolar silicate grains from this study show excesses in ^{17}O with close-to-normal $^{18}O/^{16}O$ ratios (Table 3), consistent with the definition of Group 1 grains. Group 1 is the major group for both presolar silicate and oxide grains, and is inferred to have originated from oxygen-rich low-mass (<2.5 $M_\odot$) asymptotic giant branch (AGB) stars (Nittler et al., 2008). The proposed low-mass AGB stellar origin, however, is challenged by the large ^{25}Mg excesses recently found in a number of Group 1 grains (Leitner and Hoppe, 2019); instead, origins in Type II supernovae (Leitner and Hoppe, 2019) and more massive stars (Nittler, 2019) have been proposed.

The origin of the O-anomalous oxide 022-005-2, on the other hand, is more ambiguous. Although this grain exhibits a $> 5.3\sigma$ anomaly in $\delta^{18}O$, the enrichment is quite small, ~90‰ (Table 3). The possibility of analytical artifacts in causing its ^{16}O depletion can be excluded for the following reason. All six matrix areas in C-clast 022-005 shown in Fig. 3b were measured automatically in sequence over 15 hr. The data points for the matrix areas lie perfectly along a mass-dependent fractionation line with a slope of 0.52 in Fig. 3b, which represents the effect of instrumental fractionation and/or true intrinsic variations among differ-

Table 1
Petrographic characteristics of CM- and CI-like C-clasts from Kapoeta (this study) compared to other C-clasts in HEDs and ureilites (Patzek et al., 2018a).

Clasts	Type	Size (μm)	Magnetites	Sulfides	Anhydrous silicates	Carbonates	Comment
HED (this study)							
022–005	CM-like	150 × 100					Abundant TCI clumps
024–011	CI-like	100 × 75	Aggregate, isolated	Pyrrhotite	Forsterite		Phyllosilicate-rich lithology
026–004	CI-like	50 × 25	Aggregate, isolated				
031–008	CI-like	15 × 15	Framboid		Forsterite		Magnetites are embayed against howardite pyroxene
032–011	CI-like	60 × 40	Framboid, isolated				Phyllosilicate-rich matrix
037–009	CI-like	50 × 25	Isolated				Abundant magnetite
039–006	CI-like	50 × 20	Isolated	Pyrrhotite			
039–007	CI-like	100 × 75		Pentlandite	Forsterite	Ca-carbonate	
042–002	CI-like	50 × 20	Framboid, isolated	Pyrrhotite			
042–006	CI-like	30 × 30	Framboid, aggregate, isolated				
054–002	CI-like	80 × 25	Aggregate, isolated				
060–005	CI-like	50 × 40	Aggregate				Direct contact with a CM-like clast
092–007	CI-like	50 × 25	Aggregate, isolated, plaquette				Abundant magnetite
094–007	CI-like	25 × 10	Isolated				
HED (Patzek et al., 2018a)							
	CM-like	<100–5000	Rare	Common	Chondrules and fragments	Ca-carbonate	Common TCI
	CI-like	<100–500	Common	Pyrrhotite (rare pentlandite)	Rare fragments	Rare	
Ureilites (Patzek et al., 2018a)							
	CI-like	<100–5000	Common	Pyrrhotite (rare pentlandite)	Rare fragments	Rare	

TCI = tochilinite-cronstedtite intergrowth.

Table 2
C-clasts containing oxygen- and carbon-anomalous grains.

C-clast	Type	Analyzed area (μm^2)	Presolar O-rich grains		Presolar C-rich grains	
			No.	Area[a] (μm^2)	No.	Area[b] (μm^2)
032–007	CI-like	1,047			1	0.114
039–007	CI-like	2,252	1	0.100	1	0.038
042–002	CI-like	486			2	0.430
022–005	CM-like	4,289	2	0.198		
Total	**All C-clasts**	**15,216**	**3**	**0.298**	**4**	**0.582**

a. The estimated area was based on high-resolution SE images obtained with Auger nanoprobe.
b. The estimated area was based on secondary ion images obtained with NanoSIMS.

Table 3
Oxygen isotopic ratios of O-anomalous grains (1 σ errors).

Presolar grains	Area (μm^2)	Type	Phase	Composition	$^{17}O/^{16}O$ ($\times 10^{-4}$)	$^{18}O/^{16}O$ ($\times 10^{-3}$)
039-007-1-O	0.100	Group 1	silicate	$(Mg,Fe)_{1.5}SiO_3$	5.69 ± 0.17	1.921 ± 0.028
022-005-1-O	0.072	Group 1	silicate	$(Mg,Fe)_{1.8}SiO_3$	6.54 ± 0.25	2.049 ± 0.044
022-005-2-O	0.126	Group 1	Al-rich oxide	$(Al,Fe)_2O_3$	4.17 ± 0.06	2.178 ± 0.014

Table 4
Isotopic compositions of C-anomalous grains (1 σ errors).

Presolar grains	Area (μm^2)	Type	$^{12}C/^{13}C$	$^{14}N/^{15}N$	$\delta^{29}Si$ (‰)	$\delta^{30}Si$ (‰)
032-007-1-C	0.114	MS	25.3 ± 1.0	467 ± 165	14 ± 25	45 ± 31
039-007-1-C	0.038	MS	48.9 ± 2.4	272 ± 4	-3 ± 22	-32 ± 27
042-002-1-C	0.330	MS	51.6 ± 0.3	1304 ± 137	44 ± 4	66 ± 5
042-002-2-C	0.100	MS	52.7 ± 1.6	271 ± 15	8 ± 10	22 ± 13

ent matrix areas. Note that all the matrix data were normalized to the composition of the matrix area where grain 022-005-2 is located. In comparison, grain 022-005-2 deviates from this slope-0.52 line with equal enrichments in both ^{17}O and ^{18}O. We also further verified the data point by re-measuring grain 022-005-2 using a $3 \times 3\ \mu m^2$ raster size. We will consider grain 022-005-2 as a Group 1 oxide (see discussion in Section 4.2.1).

3.2.2. Presolar carbon-rich grains

Four identified carbon-anomalous grains overlap well with mainstream (MS) presolar SiC grains from the literature in the isotope ratios of carbon, nitrogen, and silicon in Fig. 4 and therefore belong to the group of MS, which is the dominant population (~90%) of presolar SiC grains (Zinner, 2014). We were not able to accurately determine their carbon-to-silicon ratios based on our NanoSIMS data, because their carbon and silicon isotope ratios were measured during different analytical sessions (Table 4). The four grains, however, are inferred to be SiC, given their enrichments in both carbon and silicon relative to the surrounding matrix in the NanoSIMS ion images. Extensive multi-element isotopic studies revealed that MS grains originated in outflows from carbon-rich low-mass AGB stars (~1.5–3 $M_{\odot}$) with close-to-solar metallicities (e.g., Liu et al., 2018a). The carbon and nitrogen isotopic variations of mainstream grains are thought to be dominantly controlled by stellar nucleosynthesis in their parent stars (see review by Zinner, 2014 for details). In comparison, their silicon isotopic variations are mainly affected by Galactic chemical evolution (GCE) with small contributions from stellar nucleosynthesis in their parent AGB stars (e.g., Zinner, 2014; Liu et al., 2019). GCE describes the process by which the elemental and isotopic composition of a galaxy varies in time and place as a result of stellar nucleosynthesis and material cycling between stars and the interstellar medium (ISM).

3.2.3. Presolar grain abundances

Given the small sizes of the C-clasts identified in this study, it is not quite meaningful to calculate presolar grain abundances for each of the C-clasts because of large statistical uncertainties. Instead, we report the average values for all 14 C-clasts and also the 13 CI-like clasts that likely originated from the same parent body (see discussion in Section 4.1). The identified presolar silicate, oxide, and SiC grains represent an average abundance of 11^{+15}_{-7} ppm, 8^{+19}_{-7} ppm, and 38^{+30}_{-18} ppm (1σ errors), respectively, in the 14 C-clasts in our Kapoeta sample. The values change to 9^{+21}_{-8} ppm, <11 ppm, and 53^{+42}_{-25} ppm, respectively, if only the 13 CI-like C-clasts are considered. Since the two sets of values overlap within 1σ uncertainties, we will adopt the average values for the 14 C-clasts for discussion in the following sections. The abundances were calculated by dividing the area occupied by the presolar silicate, oxide or SiC grains by the total scanned matrix area across all the 14 C-clasts analyzed. Errors (1σ) were calculated by using the single-sided uncertainties reported by Gehrels

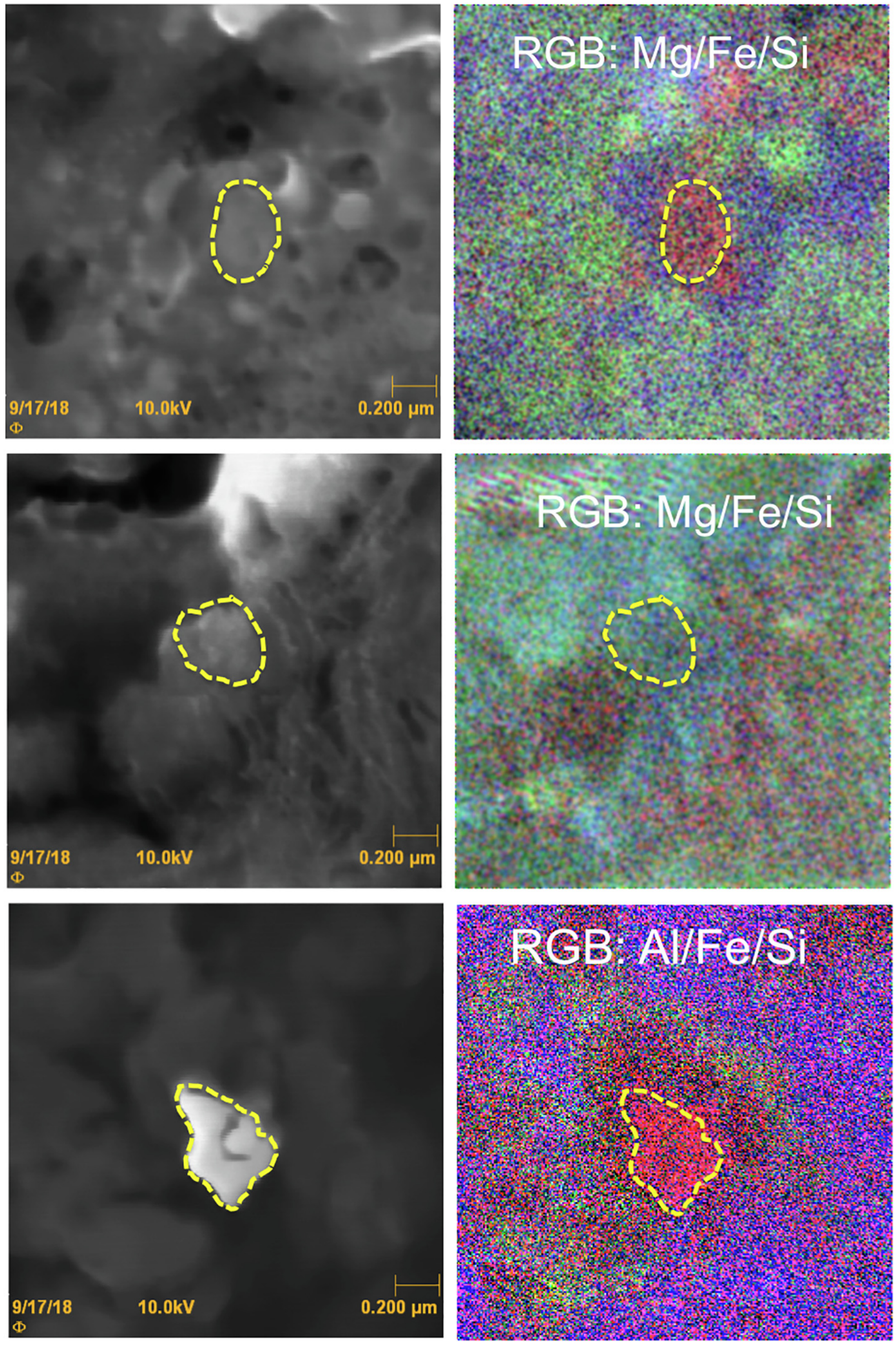

Fig. 2. Upper, middle, and lower panels show SE (left) and Auger elemental (right) images of oxygen-anomalous grain 039-007-1, 022-005-1, and 022-005-2, respectively. The grains are outlined by yellow dashed lines. (For interpretation of the references to colour in this figure legend, the reader is referred to the web version of this article.)

(1986). The upper limit of 11 ppm for presolar oxides in the 13 CI-like C-clasts was calculated for a 250 nm-sized grain.

3.3. Hydrogen, carbon, and nitrogen isotopic compositions of OM

We characterized the hydrogen, carbon, and nitrogen isotopic compositions of organic particles in a total area of ~2,000 μm^2 of fine-grained matrix-like material in three CI-like C-clasts: 024–001, 039–006, and 042–002. To characterize organic materials, we used the automatic particle definition algorithm in the L'image software to define individual C-rich region of interests (ROIs) in the carbon ion images, and calculated the corresponding carbon and nitrogen isotopic ratios. We identified 46 carbon and/or nitrogen-anomalous organic particles (with the four preso-

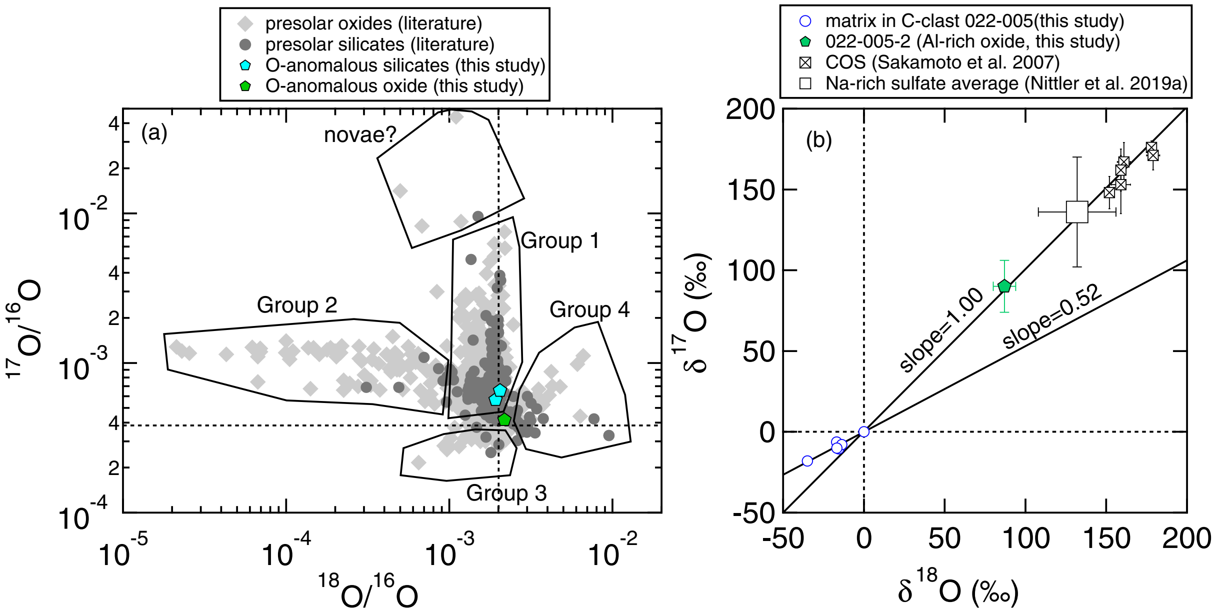

Fig. 3. (a) Oxygen three-isotope plot comparing the three oxygen-anomalous grains identified in this study with the presolar oxides and silicates reported in the literature (data source: presolar grain database, Hynes and Gyngard 2009). The group classification (black lines) is based on Nittler et al. (1997, 2008). The terrestrial ratios are shown as dashed lines. (b) Oxygen three-isotope plot in delta notation comparing oxygen-anomalous grain 022-005-2 with matrices in C-clast 022-005 and ^{16}O-poor solar objects reported in the literature. Plotted are 1σ errors.

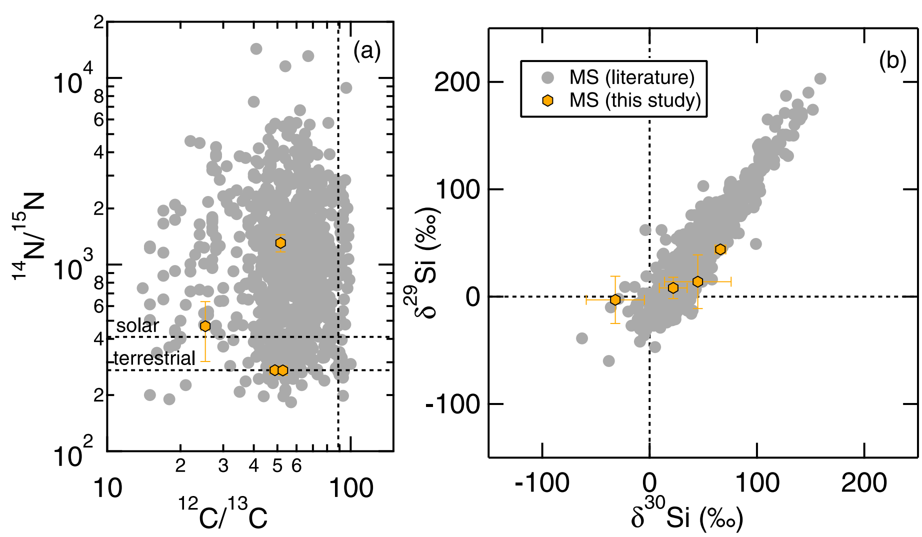

Fig. 4. Plots of (a) nitrogen versus carbon isotopes and (b) silicon three-isotopes comparing four carbon-anomalous grains identified in this study with presolar MS grains reported in the literature (data source: presolar grain database, Hynes and Gyngard, 2009). The dashed lines, unless noted, are terrestrial values. Plotted are 1σ errors.

lar SiC grains being excluded) with > 5.3σ anomalies in at least one of the carbon and nitrogen isotope ratios. The total area of the 46 organic particles corresponds to 0.38 % of the analyzed area. The data are summarized in Table 5 and compared to those of isotopically anomalous organic particles from Dominion Range (DOM) 08006 (CO3.0, Davidson et al., 2019) and Queen Alexandra Range (QUE) 99177 (CR2) in Fig. 5a. We only chose the data for these two primitive meteorites in the literature, because both the methodologies and dataset sizes are similar to those in this study. Note that although QUE 99177 is officially classified as CR2 (https://www.lpi.usra.edu/meteor/metbull.php?code=21628), several recent studies suggest that QUE 99177 is one of the most primitive CR chondrites (e.g., Floss and Stadermann, 2009) and should be classified as CR3 (Abreu and Brearley, 2010). Most of the organic particles from this study exhibit anomalies in δ^{15}N, mainly in the form of ^{15}N excesses, with small carbon

Table 5
Isotopic compositions of isotopically anomalous OM (1σ errors).

OM particle	Area (μm^2)	δ^{13}C (‰)	δ^{15}N (‰)
024-011@A1-1-01	0.119	11 ± 14	−171 ± 31
024-011@A1-1-02	0.085	36 ± 17	300 ± 40
024-011@A1-1-04	0.079	13 ± 26	−243 ± 48
024-011@A1-1-10	0.076	−37 ± 30	535 ± 67
024-011@A1-1-14	0.085	−107 ± 60	−448 ± 54
024-011@A1-4-02	0.136	55 ± 18	467 ± 29
024-011@A1-5-06	0.203	−7 ± 17	153 ± 24
024-011@A2-1-03	0.104	0 ± 26	848 ± 70
024-011@A2-1-09	0.105	6 ± 35	326 ± 65
024-011@A2-1-15	0.101	−35 ± 42	340 ± 50
024-011@A2-1-18	0.072	−247 ± 8	−125 ± 10
024-011@A2-2-01	0.169	26 ± 26	219 ± 38
024-011@A2-3-15	0.191	85 ± 14	249 ± 22
024-011@A2-3-62	0.214	35 ± 17	149 ± 23
024-011@A2-3-72	0.403	−21 ± 15	143 ± 19
024-011@A2-3-74	0.253	11 ± 19	164 ± 24
024-011@A2-3-78	0.301	5 ± 17	195 ± 22
024-011@A2-3-83	0.322	0 ± 17	163 ± 24
039-006@-1-008	0.13	−5 ± 19	314 ± 38
039-006@-1-006	0.119	−26 ± 14	−122 ± 21
039-006@-1-015	0.094	−58 ± 26	302 ± 50
039-006@-1-026	0.072	−65 ± 21	−216 ± 30
039-006@-1-302	0.15	59 ± 47	439 ± 57
039-006@-4-04	0.136	14 ± 8	105 ± 13
039-006@-4-07	0.112	23 ± 10	149 ± 18
039-006@-5-01	0.14	29 ± 16	623 ± 27
039-006@-5-02	0.52	73 ± 9	709 ± 18
039-006@-5-04	0.16	62 ± 16	821 ± 31
039-006@-5-07	0.13	20 ± 19	485 ± 30
039-006@-5-10	0.08	33 ± 25	405 ± 48
042-002@-1-01	0.145	37 ± 10	101 ± 16
042-002@-1-19	0.157	−82 ± 16	28 ± 35
042-002@-2-04	0.125	−6 ± 12	232 ± 35
042-002@-2-15	0.082	−116 ± 19	305 ± 28
042-002@-3-24	0.204	10 ± 11	202 ± 17
042-002@-3-25	0.625	1 ± 6	163 ± 10
042-002@-3-28	0.16	41 ± 13	171 ± 19
042-002@-3-40	0.259	1 ± 13	134 ± 21
042-002@-4-18	0.105	−33 ± 26	−379 ± 11
042-002@-4-49	0.125	−49 ± 20	186 ± 36
042-002@-5-008	0.359	−3 ± 8	77 ± 14
042-002@-5-009	0.211	40 ± 11	383 ± 17
042-002@-5-019	0.211	16 ± 12	177 ± 21
042-002@-5-058	0.059	−26 ± 32	494 ± 60
042-002@-5-179	0.15	9 ± 41	−256 ± 46
042-002@-5-208	0.182	−78 ± 51	−418 ± 61

isotopic anomalies (within ±∼100‰ of the solar ratio). The carbon and nitrogen isotope ratios of organic particles from the Kapoeta C-clasts overlap well with those from the DOM 08006 chondrite in Fig. 5a. On the other hand, a number of organic particles from the QUE 99177 chondrite show δ^{15}N values above 1000‰ accompanied by ^{13}C depletions, which are not seen in any of the organic particles from either the Kapoeta C-clasts or DOM 08006.

The bulk δD composition varies between 0 and 816 ‰ among the 20 matrix areas in the three C-clasts with an average of 274 ± 183 ‰ (1σ standard deviation), consistent with those previously reported for CI-like C-clasts from HED meteorites (Gounelle et al., 2005; Patzek et al., 2020). We attempted to collect correlated hydrogen isotope data in the same areas. However, it was difficult to align the carbon and nitrogen ion images with the hydrogen ion images using the SE images obtained with the NanoSIMS in the two sessions. We, therefore, separately report the hydrogen isotope data for H-rich organic particles identified by the automatic particle definition algorithm in Fig. 5b. We identified 66 D hotspots based on the > 5.3σ criterion, and most of the hotspots are submicron in size as shown in Figs. 5b and 6a. In a few cases, the D-rich organic particles appear as more diffuse regions (Fig. 6b), which may be the result of fluid action that redistributed OM (and the associated D enrichments), as previously suggested for similar large diffusion regions with ^{15}N enrichments in primitive CR3 chondrites (Floss et al., 2014). The total area of the identified isotopically anomalous organic particles corresponds to 2.0 % of the analyzed area.

4. DISCUSSION

4.1. Origins of C-clasts in kapoeta

Intriguingly, we, for the first time, observed in C-clast 031-008 (Fig. 7a-b) that magnetite framboids are embayed against a Fe-rich pyroxene (Fig. 7b), a common howardite mineral. Framboidal magnetites are secondary aqueous alteration products that are commonly found in aqueously altered chondrites (Kerridge et al., 1979). We observed extensive development of magnetite aggregates along the edge of the C-clast with a preferred orientation along the intruding host minerals (Fig. 7a-b). The majority of the magnetite aggregates are irregularly shaped and consist of numerous, tightly packed sub-μm single crystals. We also observed in C-clast 042-002 that a magnetite grain formed between its fine-grained matrix and a pigeonite grain (a howardite mineral, Fig. 7c-d). Given the apparent communication between the magnetites and the howardite host, we propose that aqueous alteration in these two C-clasts occurred after they were trapped in the regolith on Vesta, resulting in the formation of the magnetites in the C-clasts embayed with the coarse-grained host howardite minerals. In C-clast 024-011 (Fig. 7e-f), augite grains in the host howardite show irregular boundaries at contact with a phyllosilicate-rich matrix within the CI-like C-clast, indicating that the host howardite was altered by fluid from the clast. The fluid likely originated from melting of ice embedded in C-clast 024-011 as a result of its impact onto Vesta. Note that although dehydration of phyllosilicates can also release OH^- that may act in the same way as fluids to activate the aqueous alteration process, this dehydration occurs at temperatures above 400 °C (Garenne et al., 2014), which is much higher than those inferred from both Visser et al. (2018) and this study (see Section 4.2.3). Our observations above suggest that the three C-clasts contained ice mixed with fine-grained matrix-like material prior to their arrival at Vesta. This implies an ice-bearing parent body for the C-clasts in our study. This ice-bearing parent body could be a comet or an icy asteroid, given that Vesta is predicted to receive similar amounts of micro C-clasts from carbonaceous asteroids and comets (Briani et al., 2011).

Please cite this article in press as: Liu N., et al. NanoSIMS isotopic investigation of xenolithic carbonaceous clasts from the kapoeta howardite. *Geochim. Cosmochim. Acta* (2020), https://doi.org/10.1016/j.gca.2020.05.026

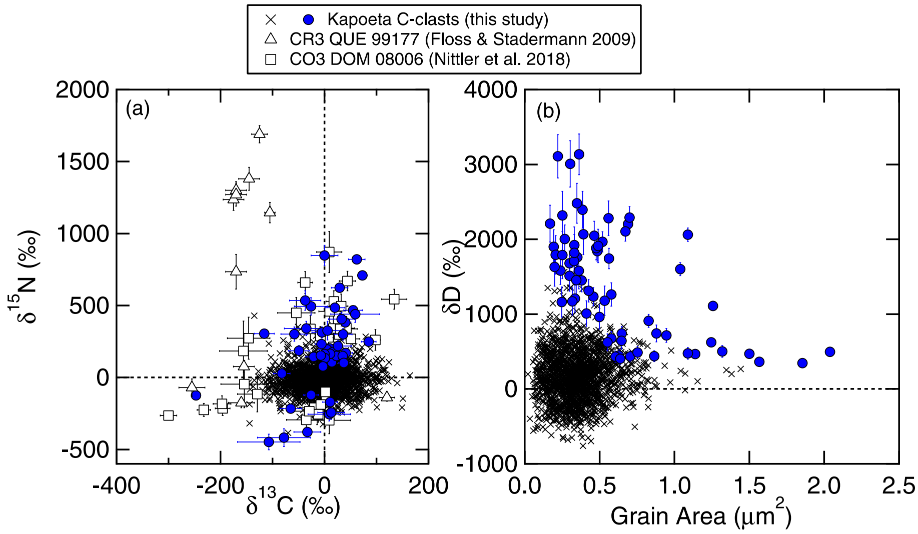

Fig. 5. (a) Nitrogen versus carbon isotope ratios of organic particles that have > 5.3σ anomalies in one or both of the isotope ratios from this study (blue circles), compared to literature data (Floss and Stadermann 2009; Nittler et al., 2018). (b) Hydrogen isotope ratio versus the grain areas of organic particles that have > 5.3σ anomalies in δD. Small black cross marks are identified organic particles whose isotopic data do not meet our criteria for being considered anomalous (see text).

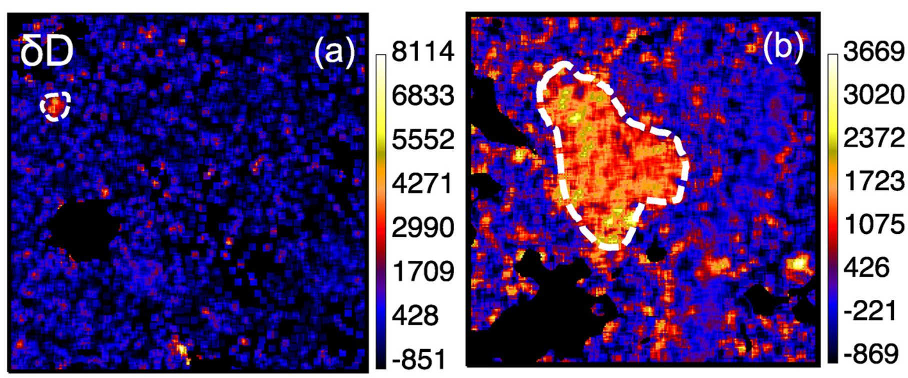

Fig. 6. δD maps of two 10 × 10 μm areas in C-clast 024-011. The D hotspots are highlighted by white dashed lines. The values in the scale are per mil.

The micro C-clasts discussed here could have experienced an earlier stage of aqueous alteration on their original parent body. Radiometric dating of aqueously formed minerals using the ^{53}Mn-^{53}Cr system ($t_{1/2} = 3.7$ Myr) is needed to identify the timing of different stages of aqueous alteration. Using the ^{53}Mn-^{53}Cr chronometer, previous studies found that aqueous alteration occurred on the parent bodies of CI, CM, and CR chondrites within the first ~10 Myr after calcium-aluminum-rich inclusion (CAI) formation (Endress et al., 1996; Hoppe et al., 2010; Petitat et al., 2011; Fujiya et al., 2012; Jilly-Rehak et al., 2014, 2017). Since micro C-clasts in howardites likely arrived at Vesta more than 1 Gyr after CAI formation (see discussion in Section 4.2.3), very young ^{53}Mn-^{53}Cr ages in secondary minerals in these micro C-clasts, compared to ages measured in carbonaceous chondrites, would be evidence for in situ aqueous alteration on Vesta from the melting of embedded water ice.

Our mineralogical characterization suggests that all of the clasts, at least the 13 CI-like C-clasts, were fragments from a single parent body and were delivered to Vesta at one time (Fig. 1a). Almost all the CI-like C-clast in our Kapoeta thin section share a similar mineralogy, characterized by similar sizes (<100 μm) and high abundances of magnetite and isolated grains of pyrrhotite (Table 1). Their mineralogies are similar to those of the CI-like clasts in HEDs previously reported by Patzek et al. (2018a, 2020) (see Table 1). Moreover, the localized distribution of the C-clasts across one edge of the sample (Fig. 1a) may indicate that all the 14 C-clasts were trapped in Vesta's regolith over a short period of time. This is also supported by the high ratio (6.5 by including the CM-like clast that was not analyzed by NanoSIMS) of CI-like to CM-like microclasts found in this study, in contrast to the ratios (0.4–1.4) previously reported for howardites (Gounelle et al., 2003). In the following sections, we will assume that the

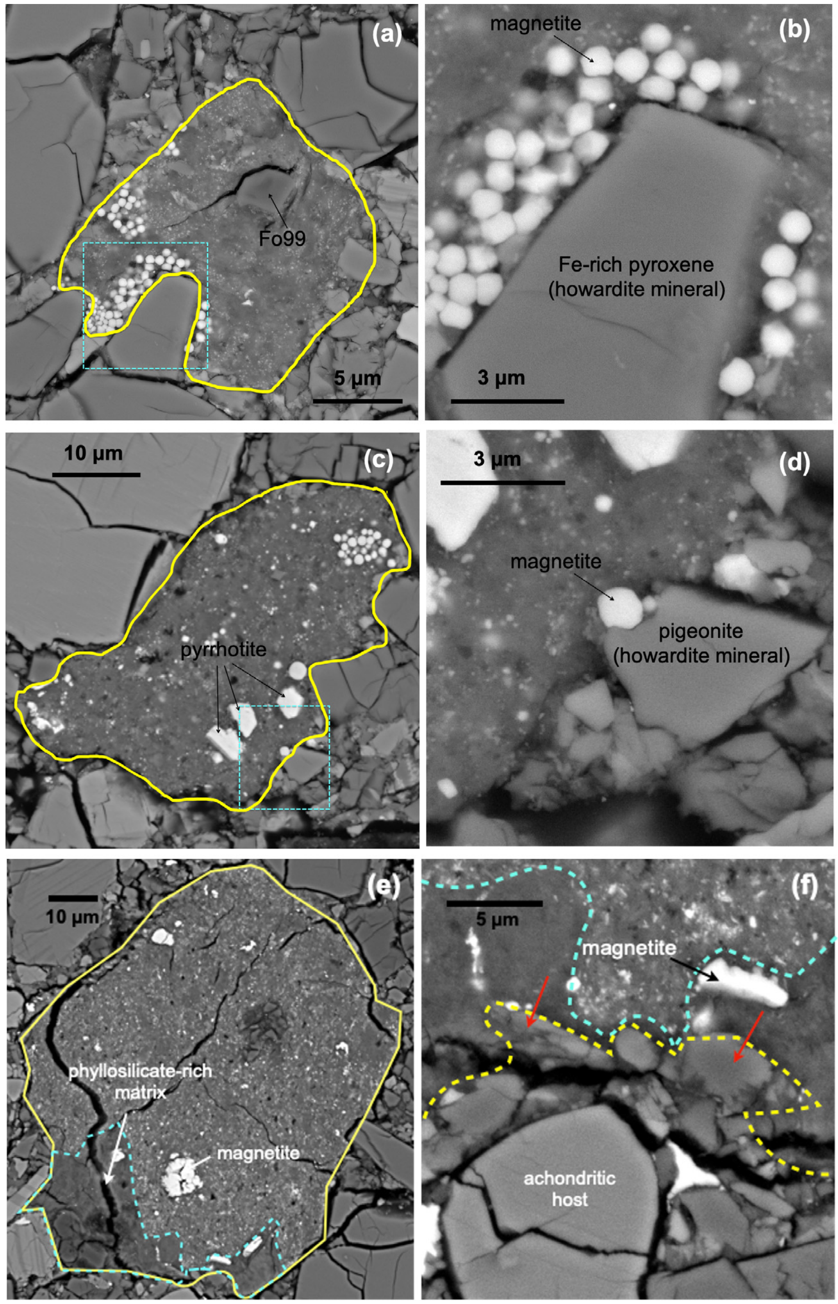

Fig. 7. (a) BSE image of CI-like C-clast 031-008 outlined by a yellow solid line. (b) A close-up of the area outlined by a blue dashed line in (a). Panels (c) and (d) show another CI-like C-clast, 042-002. (e) BSE image of CI-like C-clast 024-011 containing a highly altered lithology characterized by a phyllosilicate-rich matrix (outlined by a blue dashed line). (f) A close-up of the edge of the C-clast 024-011 from (e) showing partial dissolution of a few augite grains adjacent to the phyllosilicate-rich matrix outlined in (e) (highlighted by red arrows in panel f). (For interpretation of the references to colour in this figure legend, the reader is referred to the web version of this article.)

13 CI-like C-clasts were derived from a single parent body. Note that despite their different mineralogies, the CM-like C-clast could have also originated from the same parent body as the 13 CI-like C-clasts. Recent OSIRIS-REx images of asteroid Bennu revealed highly variable albedos across narrow local regions, which could reflect large compositional heterogeneities across a single asteroid (DellaGiustina et al., 2019). Finally, it is worth mentioning that the genetic linkage between CI-like clasts and CI chondrites is still ambiguous because of the lack of bulk oxygen isotopic data. Patzek et al. (2018b) reported some preliminary oxygen isotope data for a few CM-like and CI-like clasts: in the oxygen three-isotope plot, the data for CM-like C-clasts and CM chondrites overlap, whereas the data for CI-like C-clast and CI chondrites fall along two lines with different slopes. However, given their distinctive D/H

ratios (Patzek et al., 2020), CI-like clasts from ureilites like those studied by Patzek et al. (2018b) are probably not representative of CI-like clasts from other groups of meteorites. More importantly, based on mineralogical characterization, Alfing et al. (2019) pointed out that CI meteorites are highly brecciated and contain CI-like clasts with different mineralogies. This observation consequently suggests that a minimum mass (greater than at least several grams, e.g., Morlok et al., 2006) of CI material is needed for representative chemical and isotopic analyses, which is not feasible in the case of micro C-clasts.

4.2. Secondary processing experienced by C-clasts

4.2.1. Origin of oxygen-anomalous grain 022-005-2

The ^{16}O-poor composition of grain 022-005-2 ($\delta^{17}O = 90 \pm 16‰$, $\delta^{18}O = 86 \pm 7‰$) has been seen in a few other solar system objects, including cosmic symplectite (COS) and sodium-rich sulfates in a cometary-like carbon-rich inclusion in a CR chondrite. These objects have been linked to an ^{16}O-poor primordial water reservoir in the early solar system (Sakamoto et al., 2007; Nittler et al., 2019a). However, grain 022-005-2 is an Al-rich oxide ($(Al,Fe)_2O_3$) and likely formed at high temperatures. It is, therefore, highly unlikely that its ^{16}O-depletion is caused by isotopic exchange with this ^{16}O-poor primordial water reservoir, especially given that such ^{16}O-depletion has never been observed in minerals located within CAIs that formed at high temperatures in the protoplanetary disk (Krot, 2019). Instead, the ^{17,18}O-excesses can be explained if grain 022-005-2 originated from a low-mass AGB star with higher-than-solar metallicity. This is because the initial isotopic and elemental composition of a star is determined by the GCE. The GCE effect on oxygen isotopes is expected to increase $^{17}O/^{16}O$ and $^{18}O/^{16}O$ ratios in the Galaxy along a slope-one line over time, because ^{16}O is considered to be primary and ^{17,18}O are secondary (Clayton, 1988; Timmes and Clayton, 1996). Note that primary isotopes are isotopes that can be made in the first generation of stars, and secondary isotopes are those that cannot be made in the first generation of stars. As a result, stars of higher metallicity are expected to have higher initial $^{17}O/^{16}O$ and $^{18}O/^{16}O$ ratios than stars of lower metallicity. Thus, we consider grain 022-005-2 as a Group 1 oxide.

4.2.2. Aqueous alteration

The low presolar silicate abundance in the C-clasts in Kapoeta is consistent with the high degree of aqueous alteration inferred from their mineralogies (Section 3.1). Extensive surveys of presolar silicate abundances in different classes of meteorites have shown that presolar silicates are fragile and easily affected by secondary processing, such that they can be used as a tool to investigate nebular and parent-body processes in the early solar nebula (Floss and Haenecour, 2016). We compare our data with the literature data for presolar silicate abundances in a wide range of extraterrestrial materials in Fig. 8. Because of the large statistical uncertainties in each CR2 chondrite reported in Leitner et al. (2016), we report the average in Fig. 8 for comparison. The data points in the blue region represent the presolar silicate abundances in the most primitive extraterrestrial materials, including IDPs and several CO3.0 chondrites (Floss et al., 2006; Busemann et al., 2009; Nguyen et al., 2010; Haenecour et al., 2018; Nittler et al., 2018). In addition, the data for fine-grained chondrule rims in CO3.0, CR2, and CM2 chondrites are shown for comparison in the yellow region in Fig. 8. The destruction of presolar silicates by aqueous alteration is seen in fine-grained rims around chondrules in CO3.0 LAP 031117 (Fig. 8). The lowered presolar silicate abundance is ascribed to localized aqueous alteration in rims compared to the surrounding fine-grained matrix (Haenecour et al., 2018). Aqueous alteration seems less effective in reducing the number of presolar silicates in fine-grained chondrule rims in CR2 chondrites than in CM2 chondrites (Leitner et al., 2019), likely implying that the parent body of CR2s experienced milder aqueous alteration than the CM2 parent body. This explanation is supported by the classification of CM and CR chondrites using bulk abundances and isotopic compositions of hydrogen, carbon, and nitrogen by Alexander et al. (2013), in which CM2 chondrites are all classified as 1.1–1.9 (Murray, Yamato 791198, and Murchison classified as 1.5, 1.5, and 1.6, respectively) and CR2 chondrites all 2.0–2.6. As pointed out by Leitner et al. (2019), this explanation of the discrepancy between CM and CR chondrites seems to be challenged by the low presolar silicate abundances observed in Maribo and Paris (Leitner et al., 2019; Verdier-Paoletti et al., 2020), which are believed to be the least altered CMs (Haack et al., 2012; Hewins et al., 2014; Marrocchi et al., 2014; van Kooten et al., 2018). The current classification of the petrologic subtypes of Maribo (CM2.6, van Kooten et al., 2018) and Paris (CM2.7–2.9, Rubin, 2015), however, is based on the Rubin scale (Rubin et al., 2007), which classifies Murchison as CM2.5 and Murray CM2.4 for example, in contrast to the classification of 1.6 and 1.5, respectively, by Alexander et al. (2013). The recent bulk hydrogen data reported by Vacher et al. (2020) suggest that Maribo and Paris should be classified as CM1.9 and CM2.0–2.2, respectively, based on the scale given by Alexander et al. (2013). Note that the derived petrological scales for Maribo and Paris here should be considered as upper limits, because the bulk hydrogen contents by Vacher et al. (2020) are generally lower than those by Alexander et al. (2013), which is likely caused by degassing of their samples at higher temperatures in the former study. Thus, CM chondrites do appear to have generally experienced higher degrees of aqueous alteration than CR chondrites. In conclusion, the comparison in Fig. 8 strongly indicates that the C-clasts in Kapoeta from this study experienced high degrees of aqueous alteration (petrologic type of $<\sim 2.0$), which is, therefore, consistent with their classification as CI-like and CM-like based on their mineralogy, petrology, and carbon contents (Section 3.1).

The low presolar silicate abundance in Kapoeta C-clasts from this study agrees well with those inferred for xenolithic C-clasts in three metal-rich CB and CH chondrites (Leitner et al., 2018) but lower than the abundance in Antarctic micrometeorites (Yada et al., 2008), as shown in Fig. 8. Both xenolithic C-clasts and Antarctic microme-

Please cite this article in press as: Liu N., et al. NanoSIMS isotopic investigation of xenolithic carbonaceous clasts from the kapoeta howardite. *Geochim. Cosmochim. Acta* (2020), https://doi.org/10.1016/j.gca.2020.05.026

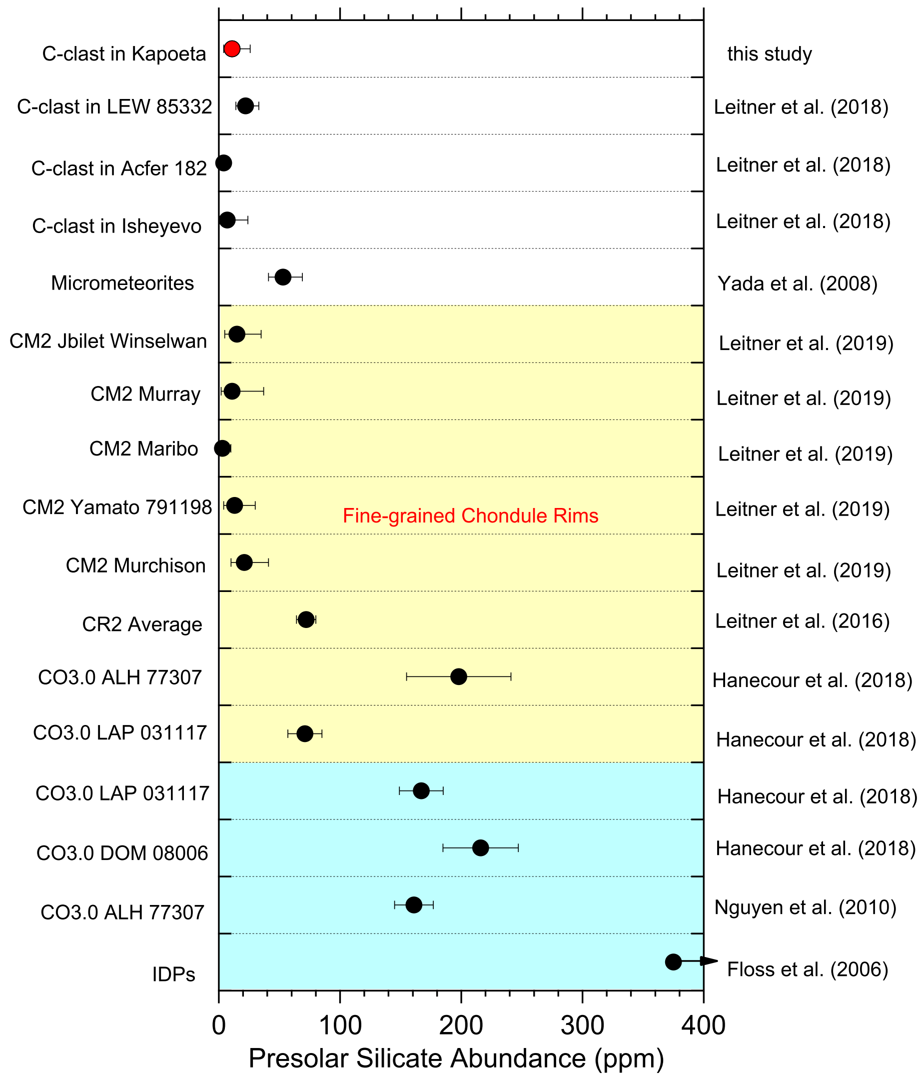

Fig. 8. Presolar silicate abundances in IDPs, meteorites, Antarctic micrometeorites, and xenolithic C-clasts. Plotted are 1σ errors. Note that the data in the yellow region are for fine-grained chondrule rims. (For interpretation of the references to colour in this figure legend, the reader is referred to the web version of this article.)

teorites are believed to originate from small debris dust formed by both asteroid collisions and comets (Nevorný et al., 2010; Briani et al., 2011). The difference is that xenolithic C-clasts are micrometeorites that landed onto the parent bodies of their host meteorites in the asteroid belt, while Antarctic micrometeorites are those that fall onto Earth in the present day. Indeed, xenolithic C-clasts and Antarctic micrometeorites are comparable in size and are dominantly composed of carbonaceous chondritic materials, which support their common origin(s). However, there are also a number of differences between xenolithic C-clasts and Antarctic micrometeorites. For instance, almost all xenolithic C-clasts can be divided into highly aqueously altered CI-like and CM-like carbonaceous materials with very few exceptions (Patzek et al., 2018a); in comparison, only ~60% of Antarctic micrometeorites are related to carbonaceous chondrites according to their mineralogy and petrology (Imae et al., 2013). Moreover, the carbonaceous-chondrite like Antarctic micrometeorites are more diverse than C-clasts: they show similarities to CM2, CR2, CV3.2, and CO3.0 (Imae et al., 2013). The higher presolar silicate abundance reported for Antarctic micrometeorites (Yada et al 2008), therefore, can be explained by the average lower degrees of aqueous alteration that Antarctic micrometeorites experienced, in comparison to the hydrated xenolithic C-clasts from Leitner et al. (2018) and this study. The different degrees of aqueous alteration experienced by micro-C-clasts and micrometeorites can be explained if (1) they had different origins (e.g., asteroids, comets), (2) their parent bodies were located at different heliocentric distances in the solar system (e.g., asteroid belt objects, Kuiper belt objects), (3) they were delivered onto Vesta and Earth at different times (e.g., varying meteoritic flux over time, e.g., Heck et al., 2017), and/or (4) hydrated xenolithic C-clasts are better preserved than other types of impacting materials on their intermediary parent bodies in the asteroid belt.

4.2.3. Thermal history

The presolar SiC and oxide abundances in the C-clasts in Kapoeta are consistent with the low amounts of heat experienced by C-clasts in other howardites inferred from Raman spectral measurements by Visser et al. (2018). The trend of decreasing presolar SiC abundance with increasing petrologic type observed in unequilibrated ordinary chondrites based on noble gas data (Huss and Lewis, 1995) demonstrated that within a meteorite class, the abundance of presolar SiC grains is primarily controlled by the degree of thermal metamorphism. The fact that the SiC abundance declines sharply for petrologic types > 3.6 further indicates that SiC is destroyed at temperatures above ~400–500 °C, the highest temperatures experienced by ordinary chondrites of petrologic type 3.6 (e.g., Cody et al., 2008; Dobrică and Brearley, 2014). The variation of presolar SiC abundances among different meteorite groups based on the bulk noble gas data, is also strongly supported by recent high-resolution NanoSIMS imaging investigation of presolar SiC grains (Davidson et al., 2014a), in which the authors reported an average abundance of ~30 ppm presolar SiC in primitive meteorites of petrologic type 3.0, CR2, and CM2 meteorites. Most of type 3.0, CM2 and CR2 chondrites experienced peak temperatures below ~200 °C (e.g., Brearley, 2006; Cody et al., 2008; Craig and Sears, 2009), although short-duration thermal metamorphism, presumably controlled by shocks or solar heating, has been reported (Nakato et al., 2008; Tonui et al., 2014; Vacher et al., 2018, 2019). On the other hand, Davidson et al. (2014a) observed that the presolar SiC abundance is significantly reduced (5^{+4}_{-2} ppm) in the Roberts Massif (RBT) 04133 CV3.4 chondrite that experienced thermal metamorphism at ~440 °C on its parent body (Davidson et al., 2014b). This observation is consistent with the conclusion based on noble gas data that SiC is destroyed at temperatures above ~400–500 °C. Fig. 9 shows that within 1σ errors the average presolar SiC abundance for the C-clasts in Kapoeta from this study is consistent with the ~30 ppm average given by Davidson et al. (2014a). In addition, the inferred presolar oxide abundance for the C-clasts from this study, ~8 ppm, is also consistent with those observed in minimally heated primitive meteorites within uncertainties (Nguyen et al., 2010; Haenecour et al., 2018; Leitner et al., 2019).

Moreover, the preservation of D hotspots in the C-clasts in Kapoeta further indicates that the peak temperature experienced by these C-clasts is quite low. Nittler et al. (2018) observed a lack of D-rich organic moieties in the matrix of the CO3.0 chondrite DOM 08006 and concluded that the very limited amount of thermal metamorphism experienced by DOM 08006 caused the loss of D-rich OM. In comparison, we observed abundant D-rich hotspots in the three C-clasts we analyzed (Fig. 5b, 6), similar to those observed in the fine-grained matrices of CM and CR meteorites by Busemann et al. (2006). In conclusion, comparison of the C-clasts from this study with meteorites of different petrologic types for their inventories of presolar grains and OM constrains the peak temperature experienced by the C-clasts to lie below ~200 °C for a long duration (on the order of millions of years following parent body accretion, e.g., Brearley and Jones, 1998), thus providing further support to the low temperatures inferred from previous Raman observations (Visser et al., 2018). Note that neither the Raman observations by Visser et al. (2018) nor the observations of presolar grains and isotopically anomalous OM from this study can exclude the possibility of flash heating to higher temperatures by shocks or solar heating experienced by xenolithic C-clasts. These C-clasts could have experienced flash heating to below 800 °C, since the recent laboratory experiments by Riebe et al. (2020) suggest that D hotspots in insoluble OM could partially survive if the temperature lies below 800 °C and lasts for only 1 s. On the other hand, the < ~200 °C constraint for a long duration, is consistent with the implication of the flash heating experiments by Riebe et al. (2020) if we translate the flash heating results to extended parent-body alteration by using the kinetic data from Cody et al. (2008) – heating above 115 °C for 10^7 yr would completely erase D hotspots in meteoritic OM.

Radiometric dating of HED meteorites using ^{40}Ar-^{39}Ar isotope systematics suggests that a single, large impact event occurred 4.48 Gyr ago and frequent energetic impact events occurred 3.4–4.1 Gyr ago, which produced significant amounts of heat to reset the Ar-Ar isotopic system (e.g., Rajan et al., 1978; Cohen 2013). The latter events occurred contemporaneously with the late heavy bombardment (Marchi et al., 2012a). It was, therefore, suggested that there was a dynamically unusual episode of bombardment in the inner solar system beginning at around 4.0 Gyr ago. Rajan et al. (1978) pointed out that more than 65% Ar loss in howardites occurs at 600–700 °C for 0.1 yr and 400–500 °C for 10 yr. The constrained low temperatures experienced by the C-clasts in the Kapoeta howardite as well as C-clasts in other groups of meteorites (Visser et al., 2018), therefore, imply that the C-clasts are likely to have been trapped in the regolith after the disappearance of these impact events. The inferred low temperatures are supported by the fact that heating primitive insoluble OM above 800 °C for 1 s completely erases D hotspots in insoluble OM (Riebe et al., 2020), in contrast to our observation of abundant D hotspots across the C-clasts from this study. Alternatively, the C-clasts could have been added onto Vestoids instead of Vesta itself, which are believed to be intermediary parent bodies of HED meteorites and probably formed about 1 Gyr ago, according to both dynamical simulations and Dawn results (Marzari et al., 1996; Nesvorný et al., 2008; Marchi et al., 2012b). Thus, the temperature constraint suggests that the C-clasts arrived at Vesta rather late, probably after ~3.5 Gyr ago.

4.3. Distribution of Circumstellar and Interstellar Materials in the Early Solar System

The results from this study support the presence of a rather homogeneous mixture of presolar grains and OM across the solar system. Fig. 9 shows that the presolar

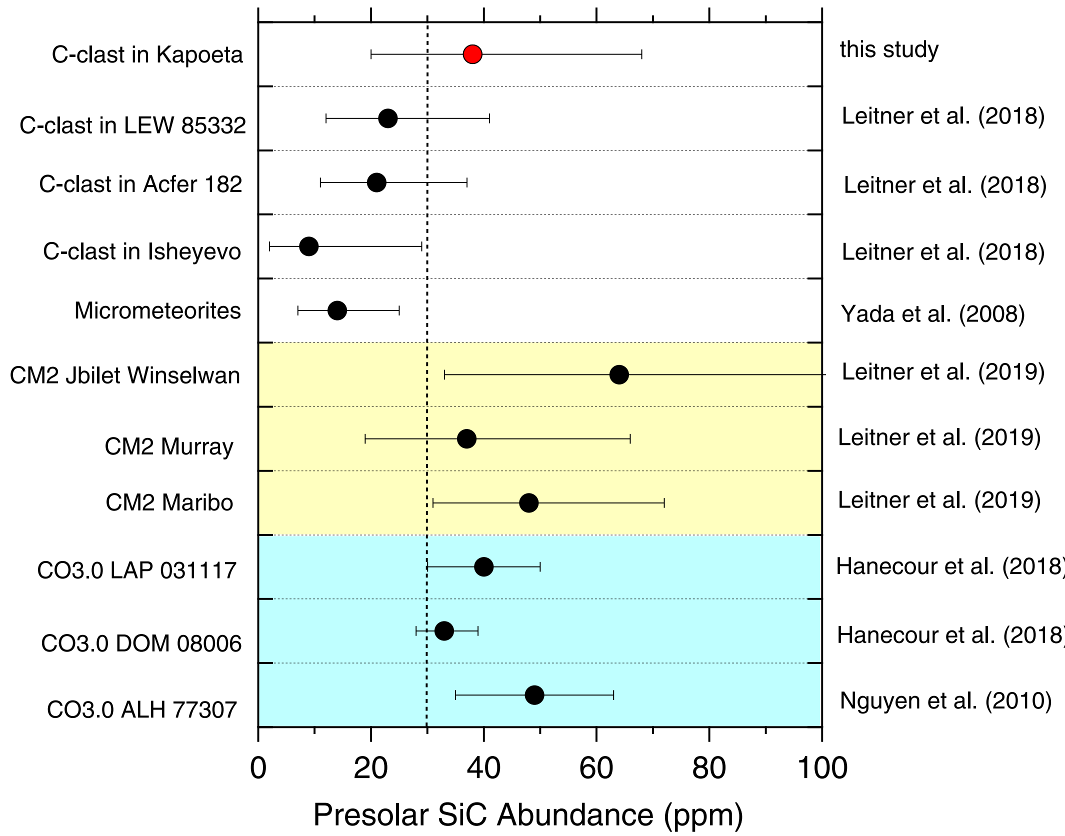

Fig. 9. Presolar SiC abundances in meteorites, Antarctic micrometeorites, and xenolithic C-clasts. The dashed line represents the CI-like presolar SiC abundance, 30 ppm, seen across different classes of primitive meteorites that have not undergone extensive parent body alteration (Davidson et al., 2014a). Plotted are 1σ errors. Note that the CM2 data from Leitner et al. (2019) were collected on fine-grained chondrule rims.

SiC abundance in the Kapoeta C-clasts is consistent with those of C-clasts in CR meteorites, micrometeorites and primitive meteorites that did not experience significant heating, and also agrees with the ~30 ppm average abundance given by Davidson et al. (2014a). In contrast, it has been suggested that both Antarctic micrometeorites (Yada et al., 2008; Floss and Haenecour, 2016) and IDPs (Floss et al., 2011) host a higher fraction of Group 4 presolar silicates that likely originated from Type II supernovae. This discrepancy could be resolved if the higher fraction of presolar supernova silicates in Antarctic micrometeorites and IDPs were caused by preservation of the isotopic heterogeneity of the parent cloud during infall and subsequent mixing and processing within the protoplanetary disk, as proposed by Burkhardt et al. (2019). Specifically, the Burkhardt et al. model suggests two periods of infall with the former rich in *r*-process material (and possibly of supernova origin) and the latter depleted of this *r*-process material; and the early infalling material transported outwards with the late infalling material being the dominant component in the inner part of the disk. As a result, this model predicts less supernova material and in turn less presolar supernova dust in the inner disk. Note that presolar supernova grains only account for a small population of presolar grains of various phases, ~ 5% by including X, AB1 and AB2 grains for presolar SiC grains (Nittler et al., 1996; Liu et al., 2016, 2018b,c; Hoppe et al., 2019), and up to 30 % by including Group 4 grains and Group 1 grains with large ^{25}Mg excesses for presolar silicates (Nittler et al., 2008; Nguyen and Messenger, 2014; Leitner and Hoppe 2019). As a result, the heterogeneous distribution of presolar supernova materials would not significantly affect the homogeneous distribution of the dominant presolar materials from other stellar sources.

If the above scenario holds true, it implies that Antarctic micrometeorites and IDPs should also contain higher abundances of presolar supernova SiC grains than primitive meteorites. However, this is difficult to test, given the small sizes of micrometeorites, in addition to the low abundances of presolar SiC grains (up to 30 ppm) and the small population of presolar supernova SiC grains (up to ~5%). One hint that may support this scenario is that a lower abundance of presolar supernova SiC grains was found in the acid residue of Qingzhen (EH3) (Lin et al., 2002), implying a heterogeneous distribution of presolar supernova materials across the solar system. Enstatite meteorites likely formed in the inner solar system, because their major constituents formed under highly reducing conditions (Ebel and Alexander, 2011), while Antarctic micrometeorites originated either from the outer solar system (if they are cometary) or the outer asteroid belt (if they are derived from C-type asteroids) (Engrand and Maurette, 1998; Nevorný et al., 2010). As a result, taking all the clues together suggests decreasing abundances of presolar supernova materials with decreasing heliocentric distance, thus supporting the Burkhardt et al. model (Burkhardt et al., 2019). As pointed out by Burkhardt et al. (2019), this hypothesis provides a coherent explanation of the isotopic dichotomy observed between non-carbonaceous-chondrite-like and carbonaceous-chondrite-like meteorites (Dauphas et al., 2004; Carlson et al., 2007; Fischer-Gödde et al., 2015; Budde et al., 2016, 2019; Burkhardt et al., 2016, 2019).

Finally, the homogeneous distribution of circumstellar and interstellar materials across the solar system is further supported by the consistent carbon and nitrogen isotopic compositions of OM from both the Kapoeta C-clasts and CO3.0 DOM 08006 (Fig. 5a). Our observation here is also consistent with the previous suggestion that all chondrites probably accreted a common organic component (Alexander et al., 2007, 2012). The ISM, molecular cloud, and the outer regions of the protoplanetary disk have been proposed as the origins of OM with large D and ^{15}N excesses, because the observed enrichments in the heavy isotopes of hydrogen and nitrogen are likely caused by isotope fractionation that occurred at extremely low temperatures. A fraction of the OM likely has an ISM origin, because the infrared and ultraviolet spectra of meteoritic insoluble OM are similar to those of refractory organics in the ISM (Pendleton et al., 1994; Cody and Alexander, 2005). On the other hand, in comparison to QUE 99177, the missing OM component with large ^{15}N-excesses ($>\sim$1000‰) and ^{13}C-depletions in the Kapoeta C-clasts and DOM 08006 is likely the result of parent-body processing, as previously suggested by Nittler et al. (2018). This suggestion is further supported by the fact that both xenolithic CI-like C-clasts in CR chondrites and CR chondrites themselves show larger D excesses, compared to other classes of meteorites and their embedded xenolithic C-clasts (Patzek et al., 2020). Note that the proposal of a common organic origin has been challenged by contrastingly different hydrogen and nitrogen isotopic compositions and their responses to varying temperatures between carbonaceous and ordinary chondrites (Alexander et al., 2007, 2010; Remusat et al., 2016). If the observed differences indeed correspond to original differences, it consequently points to a protosolar nebula with an evolving organic content as suggested by Remusat et al. (2016). However, as noted by Alexander et al. (2017), the responses of OM to different metamorphic conditions currently are not well understood and thus remain to be tested to see if it provides a coherent explanation to the differences observed between the two groups of chondrites. Finally, it is worth mentioning that the ratios of insoluble OM to circumstellar grains are quite consistent in the most primitive chondrites of each group (Alexander, 2005; Davidson et al., 2014a), in good agreement with a common OM precursor.

5. CONCLUSIONS

In this work, we studied xenolithic C-clasts in the Kapoeta howardite for their petrologic and isotopic compositions using SEM and NanoSIMS, respectively. We conclude that the identified 14 C-clasts, at least the 13 CI-like clasts, came from a single ice-bearing parent body, either an icy asteroid or a comet, originating from the outer solar system. This conclusion is based on the observations of (1) magnetites embayed between C-clasts and the howardite host minerals, (2) localized distribution of all the C-clasts, and (3) an unusually high ratio of CI-like to CM-like C-clasts. Our investigation of presolar grains and isotopically anomalous OM in the C-clasts supports their genetic linkage to carbonaceous chondrites that experienced high degrees of aqueous alteration and low amounts of heating. The inferred low degree of thermal metamorphism experienced by the C-clasts further suggests their late arrival at Vesta or Vestoids at low speeds after the late heavy bombardment occured in the inner solar system. Finally, we suggest a rather homogenous distribution of circumstellar and interstellar materials in the protoplanetary disk based on the abundances of circumstellar and interstellar materials in xenolithic C-clasts, Antarctic micrometeorites, IDPs, and primitive chondrites of different petrologic types.

Declaration of Competing Interest

The authors declare that they have no known competing financial interests or personal relationships that could have appeared to influence the work reported in this paper.

ACKNOWLEDGEMENTS

We thank Dr. J. Lewis and T. Smolar for technical support on the NanoSIMS and the Smithsonian Musesum for providing the Kapoeta thin section. We also would like to thank the associate editor Anders Meibom, Dr. C. A. Goodrich and the other two anonymous referees for providing critical reviews that significantly improved the quality of the paper. This work was supported by NASA's Emerging Worlds program (grants NNX14AG25G to RCO and 80NSSC20K0387 to NL).

RESEARCH DATA

Original data of this study are available in the supplementary file.

APPENDIX A. SUPPLEMENTARY MATERIAL

Supplementary data to this article can be found online at https://doi.org/10.1016/j.gca.2020.05.026.

REFERENCES

Abreu N. M. and Brearley A. J. (2010) Early solar system processes recorded in the matrices of two highly pristine CR3 carbonaceous chondrites, MET 00426 and QUE 99177. *Geochim. Cosmochim. Acta* **74**, 1146–1171.

Aikawa Y., van Zadelhoff G.-J., van Dishoeck E. F. and Herbst E. (2002) Warm molecular layer in protoplanetary disks. *A & A* **386**, 622–632.

Alexander C. M., O'D., Russell S. S., Arden J. W., Ash R. D., Grady M. M. and Pillinger C. T. (1998) The origin of chondritic macromolecular organic matter: a carbon and nitrogen isotope study. *Meteorit. Planet. Sci.* **33**, 603–622.

Alexander C. M., O'D., Fogel M., Yabuta H. and Cody G. D. (2007) The origin and evolution of chondrites recorded in the elemental and isotopic compositions of their macromolecular organic matter. *Geochim. Cosmochim. Acta* **71**, 4380–4403.

Alexander C. M., O'D., Newsome S. N., Fogel M. L., Nittler L. R., Busemann H. and Cody G. D. (2010) Deuterium enrichments in chondritic macromolecular material- implication for the origin and evolution of organics, water and asteroids. *Geochim. Cosmochim. Acta* **74**, 4417–4437.

Alexander C. M., O'D., Bowden R., Fogel M., Howard K. T., Herd C. D. K. and Nittler L. R. (2012) The provenances of asteroids, and their contributions to the volatile inventories of the terrestrial planets. *Science* **337**, 721–723.

Alexander C. M., O'D., Howard K. T., Bowden R. and Fogel M. L. (2013) The classification of CM and CR chondrites using bulk H, C, and N abundances and isotopic compositions. *Geochim. Cosmochim. Acta* **123**, 244–260.

Alexander C. M., O'D., Cody G. D., De Gregorio B. T., Nittler L. R. and Stroud R. M. (2017) The nature, origin and modification of insoluble organic matter in chondrites, the major source of Earth's C and N. *Geochmiestry* **77**, 227–256.

Alexander C. M. O'D. (2005) Re-examining the role of chondrules in producing the volatile element fractionations in chondrites. *Meteorit. Planet. Sci.* **40**, 943–965.

Alfing J., Patzek M. and Bischoff A. (2019) Modal abundances of coarse-grained (>5 μm) components within CI-chondrites and their individual clasts – mixing of various lithologies on the CI parent body(ies). *Geochemistry* **79** 125532.

Bischoff A., Scott E. R. D., Metzler K. and Goodrich C. A. (2006) Nature and origins of meteoritic breccias. In *Meteorites and the Early Solar System II* (eds. D. S. Lauretta and H. Y. McSween). Univ. of Arizona, Tucson, pp. 679–712.

Bischoff A., Schleiting M., Wieler R. and Patzek M. (2018) Brecciation among 2280 ordinary chondrites – constraints on the evolution of their parent bodies. *Geochim. Cosmochim. Acta* **238**, 516–541.

Bonal L., Quirico E., Flandinet L. and Montagnac G. (2016) Thermal history of type 3 chondrites from the Antarctic meteorite collection determined by Raman spectroscopy of their polyaromatic carbonaceous matter. *Geochim. Cosmochim. Acta* **189**, 312–337.

Brearley A. and Prinz M. (1992) CI chondrite-like clasts in the nilpena polymict ureilite: implications for aqueous alteration process in CI chondrites. *Geochim. Cosmochim. Acta* **56**, 1373–1386.

Brearley A. J., & Jones R. H. (1998). Chondritic Meteorites. In: Papike, J.J. (Ed.), Planetary Materials, vol. 36 Mineralogical Society of America 3: 1−398.

Brearley A. J. (2006) *The action of water*. MESS II University of Arizona Press, Tucson, pp. 584–624.

Briani G., Morbidelli A., Gounelle M. and Nesvorný D. (2011) Evidence for an asteroid-comet continuum form simulations of carbonaceous microxenolith dynamical evolution. *Meteorit. Planet. Sci.* **46**, 1863–1877.

Brownlee D., Joswiak D. and Matrajt G. (2012) Overview of the rocky component of Wild 2 comet samples: insight into the early solar system, relationship with meteoritic materials and the differences between comets and asteroids. *Meteorit. Planet. Sci.* **47**, 453–470.

Burkhardt C., Borg L. E., Brennecka G. A., Shollenberger Q. R., Dauphas N. and Kleine T. (2016) A nucleosynthetic origin for the Earth's anomalous ^{142}Nd composition. *Nature* **537**, 394–398.

Burkhardt C., Dauphas N., Hans U., Bourdon B. and Kleine T. (2019) Elemental and isotopic variability in solar system materials by mixing and processing of primordial disk reservoirs. *Geochim. Cosmochim. Acta* **261**, 145–170.

Busemann H., Young A. F., Alexander C. M. O'D., Hoppe P., Mukhopadhyay S. and Nittler L. R. (2006) Interstellar chemistry recorded in organic matter from primitive meteorites. *Science* **312**, 727–730.

Busemann H., Nguyen A. N., Cody G. D., Hoppe P., Kilcoyne D. A. L., Stroud R. M., Zega T. J. and Nittler L. R. (2009) Ultra-primitive interplanetary dust particles from the comet 26P/Grigg-Skjellerup dust stream collection. *Earth Planet. Sci. Lett.* **288**, 44–57.

Buchanan P. C., Zolensky M. E. and Reid A. M. (1993) Carbonaceous chondrite clasts in the howardites Bholghati and EET87513. *Meteoritics* **28**, 659–682.

Budde G., Burkhardt C., Brennecka G. A., Fischer-Gödde M., Kruijer T. S. and Kleine T. (2016) Molybdenum isotopic evidence for the origin of chondrules and a distinct genetic heritage of carbonaceous and non-carbonaceous meteorites. *Earth Planet. Sci. Lett.* **454**, 293–303.

Budde G., Burkhard C. and Kleine T. (2019) Molybdenum isotopic evidence for the late accretion of outer solar system material to earth. *Nat. Astron.* **3**, 736–741.

Carlson R. W., Boyet M. and Horan M. F. (2007) Chondrite barium, neodymium, and samarium isotopic heterogeneity and early earth differentiation. *Science* **316**, 1175–1178.

Clayton D. D. (1988) Isotopic anomalies: chemical memory of Galactic evolution. *Astrophys. J.* **334**, 191–195.

Craig J. and Sears D. W. G. (2009) The fine-grained matrix of the Semarkona LL3.0 ordinary chondrite: an induced thermoluminescence study. *Meteorit. Planet. Sci.* **44**, 643–652.

Cody G. D. and Alexander C. M. O'D. (2005) NMR studies of chemical structural variation of insoluble organic matter from different carbonaceous chondrite groups. *Geochim. Cosmochim. Acta* **69**, 1085–1097.

Cody G. D., Alexander C. M. O'D., Yabuta H., Kilcoyner A. L. D., Araki T., Ade H., Dera P., Fogel M., Militzer B. and Mysen B. O. (2008) Organic thermometry for chondritic parent bodies. *Earth Planet. Sci. Lett.* **272**, 446–455.

Cohen B. A. (2013) The Vestan cataclysm: impact-melt clasts in howardites and the bombardment history of 4 Vesta. *Meteorit. Planet. Sci.* **48**, 771–785.

Dauphas N., Davis A. M., Marty B. and Reisberg L. (2004) The cosmic molybdenum-ruthenium isotope correlation. *Earth Planet. Sci. Lett.* **226**, 465–475.

Davidson J. D., Busemann H., Nittler L. R., Alexander C. M. O'D., Orthous-Daunay F.-R., Franchi I. and Hoppe P. (2014a) Abundances of presolar silicon carbide grains in primitive meteorites determined by NanoSIMS. *Geochim. Cosmochim. Acta* **139**, 248–266.

Davidson J., Schrader D., Alexander C. M. O'D., Lauretta D. S., Busemann H., Franchi I. A., Greenwood R. C., Connolly, Jr, H. C., Domanik K. J. and Verchovsky A. (2014b). *Meteorit. Planet. Sci.* **49**, 2133–2151.

Davidson J., Alexander C. M. O'D., Stroud R. M., Busemann H. and Nittler L. R. (2019) Mineralogy and petrology of Dominion Range 08006: a very primitive CO3 carbonaceous chondrite. *Geochim. Cosmochim. Acta* **265**, 259–278.

De Sanctis M. C., Ammannito E., Capria M. T., Tosi F., Capaccioni F., Zambon F., Carraro F., Fonte S., Frigeri A., Jaumann R., Magni G., Marchi S., McCord T. B., McFadden L. A., McSween H. Y., Mittlefehldt D. W., Nathues A., Palomba, Pieters C. M., Raymond C. A., Russell C. T., Toplis M. J. and Turrini D. (2012) Spectroscopic characterization of mineralogy and its diversity across Vesta. *Science* **336**, 697–700.

DellaGiustina D. N., Emery J. P., Golish D. R., Rozitis B., Bennett C. A., Burke K. N., Ballouz R.-L., Becker K. J., Christensen P. R., Drouet d'Aubigny C. Y., Hamilton V. E., Reter D. C., Rizk B., Simon A. A., Asphaug E., Bandfield J. L., Barnouin O. S., Barucci M. A., Bierhaus E. B., Binzel R. P., Bottke W. F., Bowles N. E., Campins H., Clark B. C., Clark B. E., Connolly jr. H. C., Daly M. G., Leon J. de, Delbo M., Deshapriya J. D. P., Elder C. M., Fornasier S., Hergenrother C. W., Howell E. S., Jawin E. R., Kaplan H. H., Kareta T. R., Corre L. Le., Li J.-Y., Licandro J., Lim L. F., Michel P., Molaro J., Nolan M. C., Pajola M., Popescu M., Rizos Garcia J. L., Ryan A., Schwartz S. R., Shultz N., Siegler M. A., Smith P. H., Tatsumi E, Thomas C. A., Walsh K. J., Wolner C. W. V., Zou X.-D., Lauretta D. S., and The OSIRIS-REx Team. (2019). Properties of Rubble-pile Asteroid (101955) Bennu from OSIRIS-REx imaging and thermal analysis. Nat. Astron. 3: 341−351.

Dobrică E. and Brearley A. J. (2014) Widespread hydrothermal alteration minerals in the fine-grained matrices of the Tieschitz unequilibrated ordinary chondrite. *Meteorit. Planet. Sci.* **49**, 1323–1349.

Ebel D. S. and Alexander C. M. O'D. (2011) Equilibrium condensation from chondritic porous IDP enriched vapor: implications for mercury and enstatite chondrite origins. *Planet. Space Sci.* **59**, 1888–1894.

Endress M., Zinner E. and Bischoff A. (1996) Early aqueous activity on primitive meteorite parent bodies. *Nature* **379**, 701–703.

Engrand C. and Maurette M. (1998) Carbonaceous micrometeorites from Antarctica. *Meteorit. Planet. Sci.* **33**, 565–580.

Fischer-Gödde M., Burkhardt C., Kruijer T. S. and Kleine T. (2015) Ru isotope heterogeneity in the solar protoplanetary disk. *Geochim. Cosmochim. Acta* **168**, 151–171.

Floss C. (2018) Auger spectroscopy in planetary science: elemental analysis of presolar silicate grains. *Microscopy Today* **26**, 12–17.

Floss C., Stadermann F. J., Bradley J. P., Dai Z. R., Bajt S., Graham G. and Lea A. S. (2006) Identification of isotopically primitive interplanetary dust particles: a NanoSIMS isotopic imaging study. *Geochim. Cosmochim. Acta* **70**, 2371–2399.

Floss C. and Stadermann F. J. (2009) High abundances of circumstellar and interstellar C-anomalous phases in the primitive CR3 chondrites QUE 99177 and MET 00426. *Astrophys. J.* **697**, 1242–1255.

Floss C., Stadermann F. J., Mertz A. F. and Bernatowics T. J. (2011) A NanoSIMS and Auger nanoprobe investigation of an isotopically primitive interplanetary dust particle from the 55P/tempel-tuttle targeted stratospheric dust collector. *Meteorit. Planet. Sci.* **45**, 1889–1905.

Floss C. and Stadermann F. J. (2012) Presolar silicate and oxide abundances and compositions in the ungrouped carbonaceous chondrite Adelaide and the K chondrite Kakangari: the effects of secondary processing. *Meteorit. Planet. Sci.* **47**, 992–1009.

Floss C., Le Guillou C. and Brearley A. (2014) Coordinated NanoSIMS and FIB-TEM analyses of organic matter and associated matrix materials in CR3 chondrites. *Geochem. Cosmochim. Acta* **139**, 1–25.

Floss C. and Haenecour P. (2016) Presolar silicate grains: abundances, isotopic and elemental compositions, and the effects of secondary processing. *Geochem. J.* **50**, 3–25.

Fodor R. V. and Keil K. (1976) Carbonaceous and non-carbonaceous lithic fragments in the Plainview, Texas, chondrite: origin and history. *Geochim. Cosmochim. Acta* **40**, 179–189.

Formisano M., Federico C., Turrini D., Coradini A., Capaccioni F., De Sanctis M. C. and Pauselli C. (2013) The heating history of Vesta and the onset of differentiation. *Meteorit. Planet. Sci.* **48**, 2316–2332.

Fujiya W., Sugiura N., Hotta H., Ichimura K., and Sano Y. (2012). Evidence for the late formation of hydrous asteroids from young meteoritics carbonates. Nat. Commun. 3: 627 (6 pp).

Garenne A., Beck P., Montes-Hernandez G., Chiriac R., Toche F., Quirico E., Bonal L. and Schmitt B. (2014) The abundance and stability of "water" in type 1 and 2 carbonaceous chondrites (CI, CM and CR). *Geochim. Cosmochim. Acta* **137**, 93–112.

Gehrels N. (1986) Confidence limits for small numbers of events in astrophysical data. *Astrophys. J.* **303**, 336–346.

Goodrich C. A., Scott E. R. D. and Fioretti A. M. (2004) Ureilitic breccias: clues to the petrologic structure and impact disruption of the ureilite parent asteroid. *Chem. Erde* **64**, 283–327.

Goodrich C. A., Fioretti A. M. and Orman J. V. (2009) Petrogenesis of augite-bearing ureilites Hughes 009 and FRO 90054/93008 inferred from melt inclusions in olivine, augite and orthopyroxene. *Geochim. Cosmochim. Acta* **73**, 3055–3076.

Gounelle M., Zolensky M. E., Liou J.-C., Bland P. A. and Alard O. (2003) Mineralogy of carbonaceous chondritic microclasts in howardites: identification of C2 fossil micrometeorites. *Geochim. Cosmochim. Acta* **67**, 507–527.

Gounelle M., Engrand C., Alard O., Bland P. A., Zolensky M. E., Russell S. S. and Duprat J. (2005) Hydrogen isotopic composition of water from fossil micrometeorites in howardites. *Geochim. Cosmochim. Acta* **69**, 3431–3443.

Greshake A. (2014) A strongly hydrated microclast in the rumuruti chondrite NEA 6828: Implications for the distribution of hydrous material in the solar system. *Meteorit. Planet. Sci.* **49**, 824–841.

Haack H., Grau T., Bischoff A., Horstmann M., Wasson J., SØrensen A., Laubenstein M., Ott U., Palme H., Gellissen M., Greenwood R. C., Pearson V. K., Franchi I. A., Gabelica Z. and Philippe S.-K. (2012) Maribo – A new CM fall from Denmark. *Meteorit. Planet. Sci.* **47**, 30–50.

Haenecour P., Floss C., Zega T. J., Croat T. K., Wang A., Jolliff B. L. and Carpenter P. (2018) Presolar silicates in the matrix and fine-grained rims around chondrules in primitive CO3.0 chondrites: evidence for pre-accretionary aqueous alteration of rims in the solar nebula. *Geochim. Cosmochim. Acta* **221**, 379–405.

Heck P. R., Schmitz B., Bottke W. F., Rout S. S., Kita N. T., Cronholm A., Defouilloy C., Dronov A. and Terfelt F. (2017) Rare meteorites common in the ordovician period. *Nat. Astron* **1**, 1–6.

Hewins R. H., Bourot-Denise M., Zanda B., Leroux H., Barrat J.-A., Humayun M., Göpel C., Greenwood R. C., Franchi I. A., Pont S., Lorand J.-P., Cournède C., Gattacceca J., Rochette P., Kuga M., Marrocchi Y. and Marty B. (2014) The Paris meteorite, the least altered CM chondrite so far. *Geochim. Cosmochim. Acta* **124**, 190–222.

Hoppe P., MacDougall D. and Lugmair G. W. (2010) High spatial resolution ion microprobe measurements refine chronology of carbonate formation in Orgueil. *Meteorit. Planet. Sci.* **42**, 1309–1320.

Hoppe P., Leitner J. and Kodolányi J. (2015) New constraints on the abundances of silicate and oxide stardust from supernovae in the Acfer 094 meteorite. *Astrophys. J.* **808**, L9–L15.

Hoppe Pete, Stancliffe Richard J., Pignatari Marc and Amari Sachik (2019) Isotopic signatures of supernova nucleosynthesis in presolar silicon carbide grains of type AB with supersolar $^{14}N/^{15}N$ ratios. *ApJ* **887**(1), 8. https://doi.org/10.3847/1538-4357/ab521c.

Huss G. R. and Lewis R. S. (1995) Presolar diamond, SiC, and graphite in primitive chondrites: abundances as a function of meteorite class and petrologic type. *Geochim. Cosmochim. Acta* **59**, 115–160.

Huss G. R., Meshik A. P., Smith J. B. and Hohenberg C. M. (2003) Presolar diamond, silicon carbide, and graphite in carbonaceous chondrites: implications for thermal processing in the solar nebula. *Geochim. Cosmochim. Acta* **67**, 4823–4848.

Hynes K. M., and Gyngard F. (2009). The presolar grain database: http://presolar.wustl.edu/~pgd (abstract #1198) 40th Lunar and Planetary Science Conference.

Ikeda Y., Prinz M. and Nehru C. E. (2000) Lithic and mineral clasts in the Dar Al Gani (DAG) 319 polymict ureilite. *Antarct. Meteor. Res.* **13**, 177–221.

Imae N., Taylor S. and Iwata N. (2013) Micrometeorite precursors: clues from the mineralogy and petrology of their relict minerals. *Geochim. Cosmochim. Acta* **100**, 116–157.

Jilly-Rehak C. E., Huss G. R., Krot A. N., Nagashima K., Yin Q.-Z. and Sugiura N. (2014) ^{53}Mn-^{53}Cr dating of aqueously formed carbonates in the CM2 lithology of the Sutter's Mill carbonaceous chondrite. *Meteorit. Planet. Sci.* **49**, 2014–2117.

Jilly-Rehak C. E., Huss G. R. and Nagashima K. (2017) ^{53}Mn-^{53}Cr radiometric dating of secondary carbonates in CR chondrites: timescales for parent body aqueous alteration. *Geochim. Cosmochim. Acta* **15**, 224–244.

Jull A. J. T. (2001) Terrestrial ages of meteorites. In *Accretion of Extraterrestrial Matter Throughout Earth's History* (eds. B. Peucker-Ehrenbrink and B. Schmitz). Springer, Boston, MA, pp. 241–261.

Keil K., Fodor R. V., Starzyk P. M., Schmitt R. A., Bogard D. D. and Husain L. (1980) A 3.6-b.y.-old impact-melt rock fragment in the Plainview chondrite: implications for the age of the H-group chondrite parent body regolith formation. *Earth Planet. Sci. Lett.* **51**, 235–247.

Kebukawa Y., Zolensky M. E., Chan Q. H. S., Nagao K., Kilcoyne A. L. D., Bodnar R. J., Farley C., Rahman Z., Le L. and Cody G. D. (2017) Characterization of carbonaceous matter in xenolithic clasts from the Sharps (H3.4) meteorite: constraints on the origin and thermal processing. *Geochim. Cosmochim. Acta* **196**, 74–101.

Kerridge J. F., Mackay A. L. and Boynton W. V. (1979) Magnetite in CI carbonaceous meteorites: Origin by aqueous activity on a planetesimal surface. *Science* **205**, 395–397.

Krot A. N. (2019) Refractory inclusions in carbonaceous chondrites: records of early solar system processes. *Meteorit. Planet. Sci.* **54**, 1647–1691.

Leitner J., Vollmer C., Hoppe P. and Zipfel J. (2012) Characterization of presolar material in the CR chondrite Northwest Africa 852. *Astrophys. J.* **745**, 38 (16pp).

Leitner J., Vollmer C., Floss C., Zipfel J. and Hoppe P. (2016) Ancient stardust in fine-grained chondrule dust rims from carbonaceous chondrites. *Earth Planet. Sci. Lett.* **434**, 117–128.

Leitner J., Hoppe P. and Zipfel J. (2018) A study of presolar material in hydrated lithic clasts from metal-rich carbonaceous chondrites. *Meteorit. Planet. Sci.* **53**, 204–231.

Leitner J. and Hoppe P. (2019) A new population of dust from stellar explosion among meteoritic dust. *Nat. Astron.* **3**, 725–729.

Leitner J., Metzler K., Vollmer C., Floss C., Haenecour P., Kodolányi J., Harries D. and Hoppe P. (2019) The presolar grain inventory of fine-grained chondrule rims in the mighei-type (CM) chondrites. *Meteorit. Planet. Sci.*. https://doi.org/10.1111/maps.13412.

Levison H. F., Bottke W. F., Gounelle M., Morbidelli A., Nesvorný D. and Tsiganis K. (2009) Contamination of the asteroid belt by primordial trans-neptunian objects. *Nature* **460**, 364–366.

Lin Y., Amari S. and Pravdivtseva O. (2002) Presolar grains from the Qingzhen (EH3) meteorite. *Astrophys. J.* **575**, 257–263.

Liu N., Nittler L. R., Pignatari M., Alexander C. M. O'D. and Wang J. (2016a) Stellar origin of ^{15}N-rich presolar SiC grains of type AB: supernovae with explosive hydrogen burning. *Astrophys. J.* **842**, L1 (8pp).

Liu N., Gallino R., Cristallo S., Bisterzo S., Davis A. M., Trappitsch R. and Nittler L. R. (2018a) New constraints on the major neutron source in low-mass AGB stars. *Astrophy. J.* **865**(2), 112. https://doi.org/10.3847/1538-4357/aad9f3.

Liu N., Stephan T., Boehnke P., Nittler L. R., Meyer B. S., Alexander C. M. O'D., Davis A. M., Trappitsch R. and Pellin M. J. (2018b) Common occurrence of explosive hydrogen burning in type II supernovae. *Astrophys. J.* **855**, 144 (9pp).

Liu N., Nittler L. R., Alexander C. M. O'D. and Wang J (2018c) Late formation of silicon carbide in type II supernovae. *Sci. Adv.* **4**(1), eaao1054. https://doi.org/10.1126/sciadv.aao1054.

Liu N., Stephan T., Cristallo S., Gallino R., Boehnke P., Nittler L. R., Alexander C. M. O'D., Davis A. M., Trappitsch R., and Pellin M. J. Presolar Silicon Carbide Grains of Types Y and Z: Their molybdenum isotopic compositions and stellar origins. The Astrophysical Journal 881: 28 (14pp).

Lorenz C. A., Ivanova M. A., Kurat G. Brandstaetter F., FeO-rich xenoliths in the staroye pesyanoe aubrite (abstract #1612) 36th Lunar and Planetary Science Conference, 2005.

Lorenz K. A., Nazarov M. A., Kurat G., Brandstaetter F. and Ntaflos Th. (2007) Foreign meteoritic material of howardites and polymict eucrites. *Petrology* **15**, 109–125.

Marchi S., McSween H. Y., O'Brien D. P., Schenk P., De Sanctis M. C., Gaskell R., Jaumann R., Mottola S., Preusker F., Raymond C. A., Roatsch T. and Russell C. T. (2012a) The violent collisional history of asteroid 4 Vesta. *Science* **336**, 690–694.

Marchi S., Bottke W. F., Kring D. A. and Morbidelli A. (2012b) The onset of the lunar cataclysm as recorded in its ancient crater populations. *Earth Planet. Sci. Lett.* **325–326**, 27–28.

Marrocchi Y., Gounelle M., Blanchard I., Caste F. and Kearsley A. T. (2014) The paris CM chondrite: Secondary minerals and asteroidal processing. *Meteorit. Planet. Sci.* **49**, 1232–1249.

Marzari F., Cellino A., Davis D. R., Farinella P., Zappalà V. and Vanzani V. (1996) Origin and evolution of the Vesta asteroid family. *A & A* **316**, 248–262.

Messenger S. (2000) Identification of molecular-cloud material in interplanetary dust particles. *Nature* **404**, 968–971.

Messenger S., Keller L. P., Stadermann F. J., Walker R. M. and Zinner E. (2003) Samples of stars beyond the solar system: silicate grains in interplanetary dust. *Science* **300**, 105–108.

Metzler K., Bobe K. D., Palme H., Spettel B. and Stöffler D. (1995) Thermal and impact metamorphism on the HED parent asteroid. *Planet. Space Sci.* **43**, 499–525.

Mittlefehldt D. W. 1997. Achondrite Meteorites. In: Encyclopedia of Planetary Science. Encyclopedia of Earth Science. Springer, Dordrecht.

Morlok A., Bischoff A., Stephan T., Floss C., Zinner E. and Jessberger E. (2006) Brecciation and chemical heterogeneities of CI chondrites. *Geochim. Cosmochim. Acta* **70**, 5371–5394.

Nakato A., Nakamura T., Kitajima F. and Noguchi T. (2008) Evaluation of dehydration mechanism during heating of hydrous asteroids based on mineralogical and chemical analysis of naturally experimentally heated CM chondrites. *Earth Planets Space* **60**, 855–864.

Nesvorný D., Roig F., Gladman B., Lazzaro D., Carruba V. and Mothé-Diniz T. (2008) Fugitives from the Vesta family. *Icarus* **193**, 85–95.

Nesvorný D., Jenniskens P., Levison H. F., Bottke W. F., Vokrouhlick D. and Gounelle M. (2010) Cometary origin of the zodiacal cloud and carbonaceous micrometeorites. Implications for hot debris disks. *Astrophys. J.* **713**, 816–836.

Nguyen A. N., Nittler L. R., Stadermann F. J., Stroud R. M. and Alexander C. M. O'D. (2010) Coordinated analysis of presolar grains in the Allan Hills 77307 and Queen Elizabeth range 99177 meteorites. *Astrophys. J.* **719**, 166–189.

Nguyen A. N. and Messenger S. (2014) Resolving the stellar sources of isotopically rare presolar silicate grains through Mg and Fe isotopic analysis. *Astrophys. J.* **784**, 149 (15 pp).

Nittler L. R., Amari S., Zinner E., Woosley S. E. and Lewis R. S. (1996) Extinct ^{44}Ti in presolar graphite and SiC: Proof of a supernova origin. *Astrophys. J.* **462**, L31–L34.

Nittler L. R., Alexander C. M. O'D., Gao X., Walker R. M. and Zinner E. (1997) Stellar sapphires: the properties and origins of presolar Al_2O_3 in meteorites. *Astrophys. J.* **483**, 475–495.

Nittler L. R., Alexander C. M. O'D., Gallino R., Hoppe P., Nguyen A. N., Stadermann F. J. and Zinner E. (2008) Aluminum-, calcium- and titanium-rich oxide stardust in ordinary chondrite meteorites. *Astrophys. J.* **682**, 1450–1478.

Nittler L. R. and Ciesla F. (2016) Astrophysics with extraterrestrial materials. *Ann. Rev. Astron. Astrophys.* **54**, 53–93.

Nittler L. R., Alexander C. M. O'D., Davidson J., Riebe M. E. I., Stroud R. M. and Wang J. (2018) High abundances of presolar grains and ^{15}N-rich organic matter in CO3.0 chondrite Dominion Range 08006. *Geochim. Cosmochim. Acta* **226**, 107–131.

Nittler L. R., Stroud R. M., Trigo-Rodríguez J. M., De Gregorio B. T., Alexander C. M. O'D., Davidson J., Moyano-Cambero C. E. and Tanbakouei S. (2019a) A cometary building block in a primitive asteroidal meteorite. *Nat. Astron.* **3**, 659–666.

Nittler L. R., Stroud R. M., Alexander C. M. O'D. and Howell K. (2019b) Presolar grains in primitive ungrouped carbonaceous chondrite Northwest Africa 5958. *Meteorit. Planet. Sci., in press*. https://doi.org/10.1111/maps.13397.

Nittler L.R. (2019). Isotopic imprints of super-AGB stars and their supernovae in the solar system (abstract #6424). 82nd Annual Meeting of The Meteoritical Society in Sapporo, Japan.

Nozette S. and Wilkening L. L. (1982) Evidence for aqueous alteration in a carbonaceous xenolith from the Plainview (H5) chondrite. *Geochim. Cosmochim. Acta* **46**, 557–563.

Pendleton Y. J., Sandford S. A., Allamandola L. J., Tielens A. G. G. M. and Sellgren K. (1994) Near-infrared absorption spectroscopy of interstellar hydrocarbon grains. *Astrophys. J.* **437**, 683–696.

Patzek M., Bischoff A., Visser R. and John T. (2018a) Mineralogy of volatile-rich clasts in brecciated meteorites. *Meteorit. Planet. Sci.* **53**, 2519–2540.

Patzek M., Pack A., Bischoff A., Visser R., and John T. (2018b). O-isotope composition of CI- and CM-like clasts in ureilites, HEDs, and CR chondrites. (abstract #6254). 81st Annual Meeting of The Meteoritical Society in Moscow, Russia.

Patzek M., Hoppe P., Bischoff A., Visser R. and John T. (2020) Hydrogen isotopic composition of CI- and CM-like clasts from meteorite breccias−Sampling unknown sources of carbonaceous chondrite materials. *Geochim. Cosmochim. Acta* **272**, 177–197.

Pearson V. K., Septhton M. A., Franchi I. A., Gibson J. M. and Gilmour I. (2006) Carbon and nitrogen in carbonaceous chondrites: elemental abundances and stable isotopic composition. *Meteorit. Planet. Sci.* **41**, 1899–1918.

Petitat M., Marrocchi Y., Mckeegan K. D., Mostefaoui S., Meibom A., Zolensky M. E. and Gounelle M. (2011) ^{53}Mn-^{53}Cr ages of Kaidun carbonates. *Meteorit. Planet. Sci.* **46**, 275–283.

Prasad M. S., Rudraswami N. G. and Panda D. K. (2013) Micrometeorite flux on Earth during the last ∼50,000 years. *J. Geophys. Res. Planets* **118**, 2381–2399.

Pun A., Keil K., Taylor G. J. and Wieler R. (1998) The Kapoeta howardite: implications for the regolith evolution of the howardite-eucrite-diogenite parent body. *Meteorit. Planet. Sci.* **33**, 835–851.

Rajan R. S., Huneke J. C., Smith S. P. and Wasserburg G. J. (1978) Argon 40-argon 39 chronology of lithic clasts from the Kapoeta howardite. *Geochim. Cosmochim. Acta* **43**, 957–971.

Remusat L., Piani L. and Bernard S. (2016) Thermal recalcitrance of the organic D-rich component of ordinary chondrites. *Earth Planet. Sci. Lett.* **435**, 36–44.

Riebe M. E. I., Foustoukos D. I., Alexander C. Mo. O'D., Steele A., Cody G. D., Mysen B. and Nittler L. R. (2020) The effects of atmospheric entry heating on organic matter in interplanetary dust particles and micrometeorites. *Earth Planet. Sci. Lett.* **540** 116266.

Rubin A. E., Trigo-Rodríguez J. M., Huber H. and Wasson J. T. (2007) Progressive aqueous alteration of CM carbonaceous chondrites. *Geochim. Cosmochim. Acta* **71**, 2361–2382.

Rubin A. E. and Bottke W. F. (2009) On the origin of shocked and unshocked CM clasts in H-chondrite regolith breccias. *Meteorit. Planet. Sci.* **44**, 701–724.

Rubin A. E. (1989) An olivine-microchondrule-bearing clast in the Krymka meteorite. *Meteoritics* **24**, 191–192.

Rubin A. E. (2015) An American on Paris: extent of aqueous alteration of a CM chondrite and the petrography of its refractory and amoeboid olivine inclusions. *Meteorit. Planet. Sci.* **50**, 1595–1612.

Sakamoto N., Seto Y., Itoh S., Kuramoto K., Fujino K., Nagashima K., Krot A. N. and Yurimoto H. (2007) Remnants of the early solar system water enriched in heavy oxygen isotopes. *Science* **317**, 231–233.

Slodzian G., Hillion F., Stadermann F. J. and Zinner E. (2014) QSA influences on isotopic ratio measurements. *Appl. Surf. Sci.* **231–232**, 874–877.

Stadermann F. J., Floss C., Bose M. and Lea A. S. (2009) The use of Auger spectroscopy for the in situ elemental characterization of sub-micrometer presolar grains. *Meteorit. Planet. Sci.* **44**, 1033–1049.

Timmes F. X. and Clayton D. D. (1996) Galactic evolution of silicon isotopes: application to presolar SiC grains from meteorites. *Astrophys. J.* **472**, 723–741.

Tonui E., Zolensky M., Hiroi T., Nakamura T., Lipschutz M. E., Wang M.-S. and Okudaira K. (2014) Petrographic, chemical and spectroscopic evidence for thermal metamorphism in carbonaceous chondrites I: CI and CM chondrites. *Geochim. Cosmochim. Acta* **126**, 284–306.

Vacher L. G., Marrocchi Y., Villeneuve J., Verdier-Paoletti M. J. and Gounelle M. (2018) Collisional and alteration history of the CM parent body. *Geochim. Cosmochim. Acta* **239**, 213–234.

Vacher Lionel G., Piralla Maxim, Gounelle Matthie, Bizzarro Marti and Marrocchi Yve (cher et al.,) Thermal evolution of hydrated asteroids inferred from oxygen isotopes. *Astrophys. J.* **882**(2), L20. https://doi.org/10.3847/2041-8213/ab3bd0.

Vacher L. G., Piani L., Rigaudier T., Thomassin D., Florin G., Piralla M. and Marrocchi Y. (2020) Hydrogen in chondrites: influence of parent body alteration and atmospheric contamination on primordial components. *Geochim. Cosmochim. Acta* **281**, 53–66. https://doi.org/10.1016/j.gca.2020.05.007.

van Kooten E. M. M. E., Cavalcante L. L., Nagashima K., Kasama T., Balogh Z. I., Peeters Z., Hsiao S. S.-Y., Shang H., Lee D.-C., Lee T., K.A.N. and Bizzarro M. (2018) Isotope record of mineralogical changes in a spectrum of aqueously altered CM chondrites. *Geochim. Cosmochim. Acta* **237**, 79–102.

Verdier-Paoletti M. J., Nittler L. R., and Wang J. (2020). New estimation of presolar grain abundances in the Paris meteorite (abstract #2523). 51st Lunar and Planetary Science Conference.

Vernazza P., Marsset M., Beck P., Binzel R. P., Birlan M., Brunetto R., Demeo F. E., Djouadi Z., Dumas C., Merouane S., Mousis O. and Zanda B. (rnazza et al.,) Interplanetary dust particles as samples of icy asteroids. *Astrophys. J.* **806**(2), 204 (10pp). https://doi.org/10.1088/0004-637X/806/2/204.

Visser R., John T., Menneken M., Patzek M. and Bischoff A. (2018) Temperature constraints by Raman spectroscopy of organic matter in volatile-rich clasts and carbonaceous chondrites. *Geochim. Cosmochim. Acta* **241**, 38–55.

Walsh K. J., Morbidelli A., Raymond S. N., O'Brien D. P. and Mandell A. M. (2011) A low mass for mars from Jupiter's early gas-driven migration. *Nature* **475**, 206–209.

Weisfeiler M., Turcotte D. L. and Kellogg L. H. (2017) Modeling the early evolution of Vesta. *Meteorit. Planet. Sci.* **52**, 859–868.

Wilkening L. L. (1973) Foreign inclusions in stony meteorites – I. carbonaceous chondritic xenoliths in the Kapoeta howardite. *Geochim. Cosmochim. Acta* **37**, 1985–1989.

Yada T., Floss C., Stadermann F. J., Zinner E., Nakamura T., Noguchi T. and Lea A. S. (2008) Stardust in Antarctic micrometeorites. *Meteorit. Planet. Sci.* **43**, 1287–1298.

Zinner E. (2014). Presolar grains. In Meteorites and cosmochemical processes, edited by Holland H. D. and Turekian K. K. Treatise on geochemistry (ed. A. M. Davis) vol. 2, 2nd ed. Oxford: Elsevier-Pergamon. pp. 181–213.

Zolensky M. E., Hewins R. H., Mittlefehldt D. W., Lindstrom M. M., Xiao X. and Lipschutz M. E. (1992) Mineralogy, petrology and geochemistry of carbonaceous chondritic clasts in the LEW 85300 polymict eucrite. *Meteoritics* **27**, 596–604.

Zolensky M. E., Weisberg M. K., Buchanan P. C. and Mittlefehldt D. W. (1996) Mineralogy of carbonaceous chondrite clasts in HED achondrites and the Moon. *Meteorit. Planet. Sci.* **31**, 518–537.

Associate editor: Anders Meibom